Experimental and computational devices on the way to quantum-dot based light-emitting electrochemical cells

Master thesis Materials Science and Engineering
Performed at the TU Delft
Reinout Floris Ubbink
4401433
Supervisors: Maryam Alimoradi Jazi,
Arjan Houtepen, Arjan Mol
06-09-2020

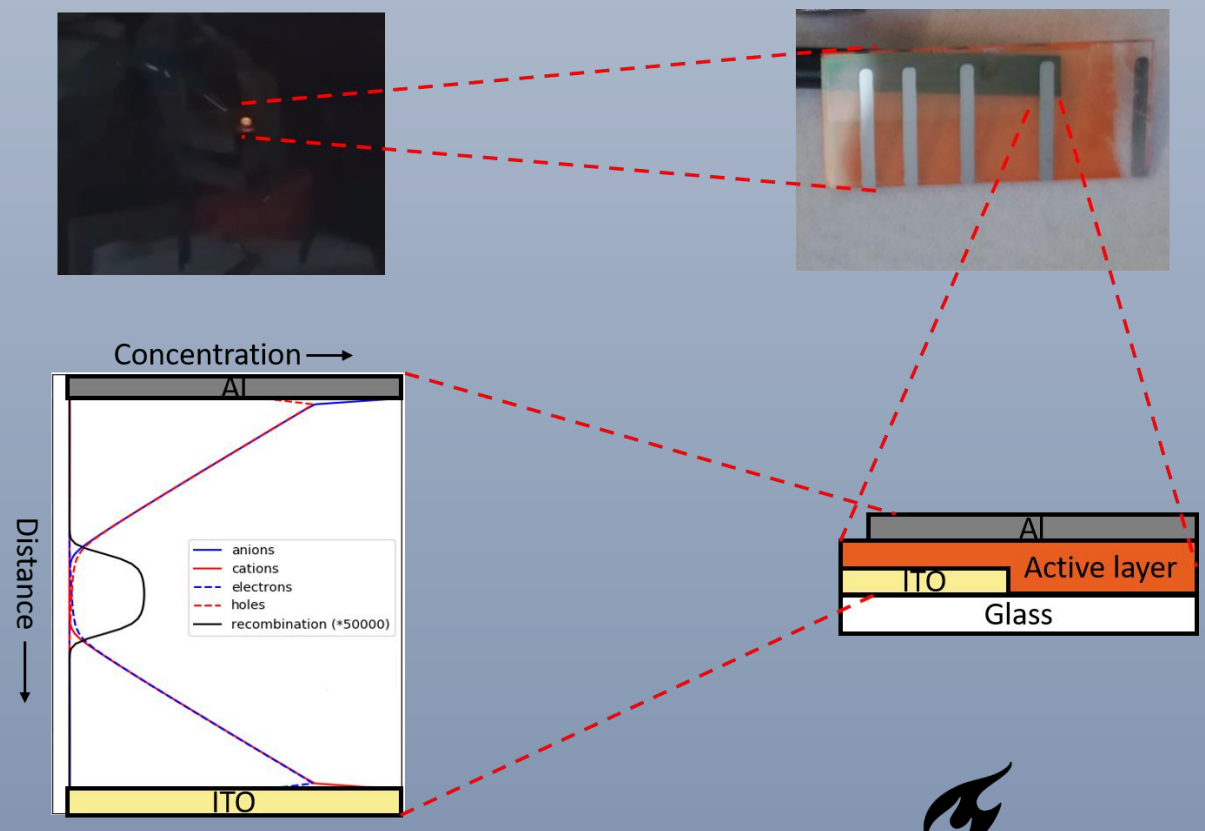

TU Delft

Table of contents

Abstract

Due to their simple structure and the possibility for *in situ* doping, light emitting electrochemical cells (LECs) are shaping up to be a cheap and easily produced alternative to LEDs. To date, little research has been done to combine the luminescent properties of colloidal quantum dots (QDs) with the LEC concept. In this thesis, steps are taken towards developing a QD-based LEC. The LECs were produced based on the semiconducting polymer MEH-PPV, ZnO and CdSe/CdS/ZnS quantum dots. Furthermore, drift-diffusion simulations were performed to discover general trends in LECs. MEH-PPV devices performed as expected. ZnO QDs were found to be unsuitable for LECs due to their high intrinsic conductivity and low luminescence efficiency, while CdSe/CdS/ZnS QDs were identified as promising candidates. Results from the drift-diffusion simulations suggested that unlike in LEDs, the type of electrode material has little effect on device operation. Charge carrier mobility was identified as the limiting parameter for luminescence intensity. It is thus suggested that improving carrier mobility in QD films is the most important step towards QD-based LECs.

Introduction

The rise of semiconductor materials has, among other important developments, led to a revolution in lightning technologies. Semiconductor based light emitting diodes (LEDs) have been around since the sixties, but only in the last two decades have taken over as the new widespread standard for lighting, due to their high efficiency. In most ambient lighting lamps, inorganic bulk semiconductor materials are used while in displays polymer-based LEDs are the standard. In these organic LEDs, known as OLEDs, semi-conducting conjugated polymers are used as the light-emitting material, which allows for the production of flexible and ultrathin displays.

Because each pixel emits its own light through electroluminescence, OLED screens can display more contrast, brighter colours and deeper blacks than backlit liquid crystal displays (LCDs), where only a single lamp is used and each pixel can be set to either transmit or block this light. Despite their success in screens, widespread use of OLEDs has been hampered by their high production costs, inferior lifetime and efficiency compared to the traditional inorganic LEDs. The reason for their high cost is the complicated multilayer design necessary to make them work. Up to 9 different thin-layer materials (electrodes not included) need to be stacked to make an OLED, and all of these must be deposited without damaging the layers already being present.

An alternative which is much easier to produce is the light-emitting electrochemical cell (LEC). In this design, first discovered by Pei et al.[1], a semiconducting polymer is combined with an electrolyte, which allows for *in situ* doping of the semiconductor and easy injection of charge carriers, eliminating the need for complex multilayer structures. Although LECs can be based on ionic transition metal complexes (iTMS) as well[2], the focus in this project is on LECs that use a semiconductor as their emissive material. The semiconducting polymers that are used in LECs have a number of drawbacks such as high production cost and low luminescence efficiency. Since mobility of the ions is crucial for LEC operation, bulk semiconductors cannot be used. However, it may still be possible to combine some of the properties of inorganic semiconductors with the LEC design by using semiconductor nanocrystals (NCs). Semiconductor NCs, also called quantum dots (QDs) can be produced more quickly and easily than semiconducting polymers[3]. In addition to this, they show very sharp emission and can achieve near unity photoluminescence quantum yields [4, 5], and are therefore prime candidates for use in luminescent devices.

Although “quantum light emitting diode” (QLED) screens are already commercially available, the nanoparticles in them are only used as phosphors and need a UV backlight to operate. Actual electroluminescence can be observed in QDLEDs, which are a lot like OLEDs except the light-emitting

polymer has been replaced with NCs[6]. Undoped QDs however are not very conductive, so only a very thin layer of dots (~3 monolayers) can be used in these devices. Additionally, hole- and electron transport layers are needed to allow the injection of charge carriers into the QDs[6]. In LECs, electric double layers of ions at the interface eliminate the need for transport layers.

One disadvantage of QDs is that doping them can lead to negative side effects: extra states introduced in the lattice and especially the surface of the nanocrystals by dopants can make the QDs unstable or create traps for electrons or holes, impeding the quantum yield and conductivity[7, 8]. Quantum dots can however also be doped electrochemically in the presence of ions, similar to the operating process of a LEC[9], without these negative side effects. The question is then if it is possible to produce a LEC using quantum dots as the light-emitting material. Because of the electrochemical doping, more excess electrons and holes would be present in the QDs. This would lead to improved conductivity in the doped regions, which would allow the use of thicker quantum dot films. Compared to current LECs, the colour sharpness and chemical stability could be improved while maintaining the simple design by replacing the polymer with quantum dots.

In this master thesis, steps are taken towards developing a quantum dot-based LEC. A brief overview of relevant theoretical concepts is given in chapter 2. Chapter 3 is devoted to the experimental and computational details of the thesis. In chapter 4, results of experiments on LEC devices based on polymers and two types of quantum dots are discussed. The current-voltage (known as I-V) and luminescence characteristics of polymer-based MEH-PPV LECs are compared with those found in literature. I-V curves obtained from LEC films based on ZnO and CdSe/CdS/ZnS quantum dots are also presented. Then in Chapter 5 the results from computational simulations are discussed. These include concentration profiles and band structures of LEC devices with different parameters at steady state, as well as transient current density and recombination curves. The I-V curve of a device was also simulated and is compared with the experimental results. Based on these results, theoretical predictions for the trends in LEC are that carrier mobility directly affects the luminescence intensity, electrode material choice has little impact on device operation and a higher ion concentration can lead to more heavily doped regions and thus higher current densities and luminescence intensities. Finally, based on both the experimental and computational results, recommendations and directions for future research and development of quantum dot LECs are given in chapter 6.

Theoretical background

In this chapter the theoretical concepts relevant to LECs are discussed. Section 2.1 is intended as a recap of my understanding of semiconductor theory. While all of it is common knowledge, I still found it useful to include as this entire thesis is built around these concepts, and I will repeatedly refer to them. Should the reader ever find themselves lost or unable to understand my decisions or conclusions, this section can be referred upon. In section 2.2 the theory behind colloidal quantum dots is discussed. Section 2.3 explains the concept and theory of LECs themselves.

2.1 Semiconductors

Metals combine a set of properties that is very hard to replicate in other materials, such as strength, toughness, durability and the ability to conduct heat and electricity. Most of these are due to chemical uniformity on an atomic scale: in a bulk metal lattice, many atoms share similar or even identical d- and f-orbitals, forming bonds which are neither covalent nor ionic in nature. Instead, the atomic orbitals split into extremely delocalized orbitals (often called "states"), which are shared by all atoms in the crystal lattice. This model is called the linear combination of atomic orbitals (LCAO). Due to the Pauli exclusion principle, each of these states has a different energy level than the others, but because there are so many states, the difference in energy between two adjacent states is very small and a so-called energy band of available states is formed (Figure 2.1).

Electrons can move freely from state to state as long as there is no other electron in it (Pauli exclusion) and the energy difference between the levels is small compared to *kT,* which is always the case in metals due to the large number of atoms (and thus states) contributing in the lattice. Typically, a continuous energy band of states is only partially filled up with electrons which leaves many states unoccupied. These easily accessible free states are what allows electric conduction in metals. If there are no available free states, as is the case in insulators, electrons cannot be accelerated and are stuck in place, either in local covalent bonds or in even more local atomic orbitals. However, besides insulators and electrical conductors, a third group of compounds can be distinguished: semiconductors. Semiconductor materials have the same spread-out shared orbitals as metals do, which in practice means semi-conductors are either crystalline solids or polymers. The key difference however is that semiconductors have not one continuous band of energy levels but two, with a "band gap" in between (Figure 2.1). In this band gap, there are no available energy states because the electrons are forbidden by quantum rules to occupy that specific energy. The two continuous energy bands below and above the band gap are called the valence and conduction band, respectively. In the intrinsic state, only the valence band is filled up with electrons, while the conduction band is empty.

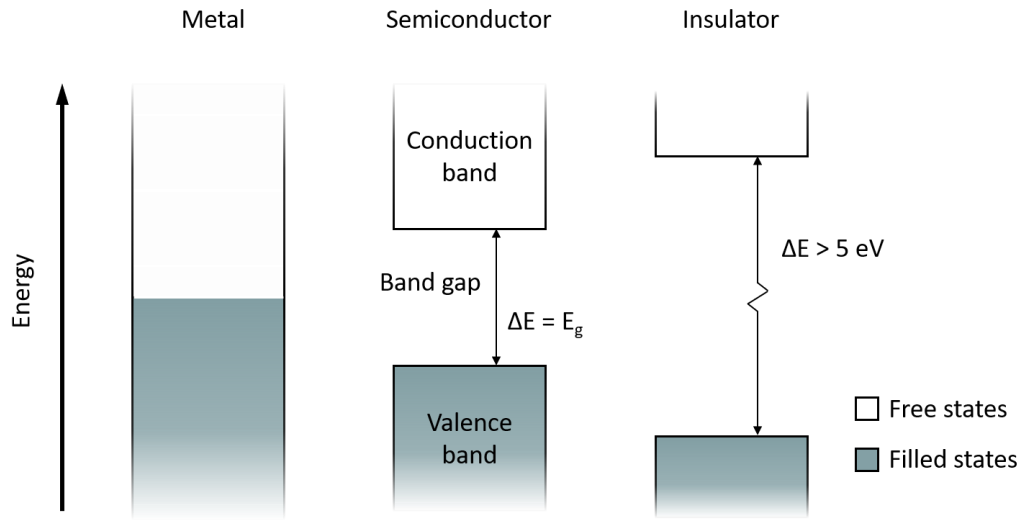

Figure 2.1 Comparison of band structure in metals, semiconductors and insulators. If a material has a continuous but partially filled band of states it is an electrical conductor. Materials with "band gaps" larger than 5 eV are typically considered insulators, while materials with a lower bandgap are semiconductors. Electrons are only mobile when they can freely access unoccupied states.

Crystalline silicon is the most famous and widespread semiconductor. Due to the half-filled p-shell of silicon, it can form diamond crystal lattices with an equal amount of bonding orbitals (which form the valence band) and antibonding orbitals (which form the conduction band). Semiconductors can also be formed by combining equal molar amounts of elements from group III and V (often called III-V semiconductors) or even group II and VI. These compounds can form diamond-like zinc-blende or wurtzite crystal lattices where the average amount of valance electrons is that is available per atom is the same as in silicon, since half of the atoms has one/two less and half one/two more valence electrons. The combined valence electrons from both elements result in a band structure much like that of silicon, with a filled valence band and an equally large but empty conduction band. Band gaps in these materials differ depending on the specific elements that are used to make them. In this project, a few variations of II-VI semiconductors are used.

Semiconductors are not fully insulating at room temperature, since a certain fraction of electrons is in the conduction band at any time due to thermal excitation. The higher the temperature, the more electrons will be excited to the conduction band, and the lower the specific resistance of a semiconductor will become. Electrons can also be excited to the conduction band in other ways, e.g. by absorption of a photon with sufficiently high energy. Since charge neutrality must be preserved, whenever an electron is excited to the conduction band, a free state is left behind in the valence band. These free states can be thought of as particles as well, and are called holes. While holes have positive charge, they can 'move' through the lattice when neighbouring electrons continuously hop into the hole. Both electrons in the conduction band and holes in the valence band contribute to electrical conduction in the semiconductor.

2.1.1 Electron/hole recombination

Excited electrons in the conduction band can recombine with a hole in the valence band, so that both particles are annihilated while energy equal to that of the band gap is released in the process. This can happen in 3 different ways: radiative, Auger and defect recombination (Figure 2.2). During radiative recombination energy is released in the form of a photon, which is then emitted from the lattice. The larger the band gap, the more energy is released, which translates to shorter wavelengths of the photons and colours more towards the violet side of the spectrum. Auger recombination occurs when an electron transfers its recombination energy to another electron in the conduction band, exciting it "higher" into the band. This second electron then quickly relaxes to the edge of the conduction band, releasing the excess energy as heat.

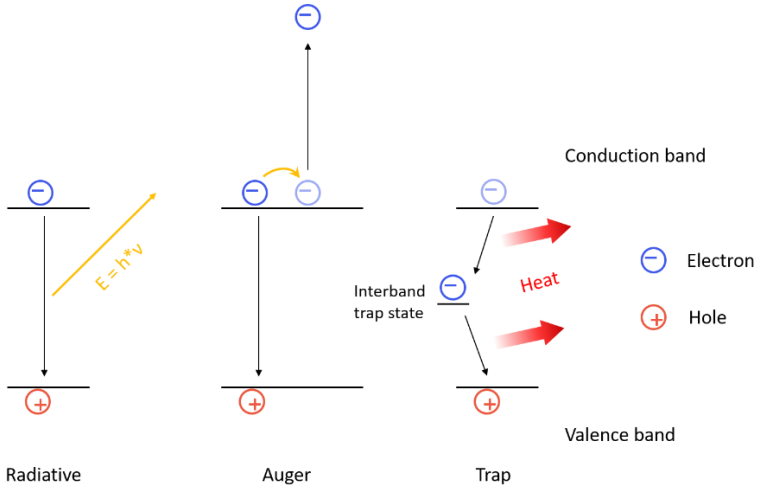

Figure 2.2. Comparison of the different types of recombination. In radiative recombination, energy is released by emission of a photon. In an Auger process, energy gained by an electron falling back to the conduction band is transferred to another electron in the valence band. This excess energy is then quickly released as heat. In trap recombination, a trap state in between the valence and conduction band is occupied by a hole or electron, after which this trapped charge carrier recombines. The energy is released as heat in two steps.

Crystal lattices always contain some defects, be they vacancies, interstitials or impurities, and polymers contain impurities as well. These defects introduce states in between the band edges called trap states. Electrons (or holes) can occupy such a trap state before recombining. The energy is then released in multiple steps to the lattice in the form of heat. For most applications, light emitting devices included, trap state recombination interferes with the intended process, and thus defects and impurities must be avoided whenever possible.

2.1.2 Doping in semiconductors

In crystalline semiconductors some of the lattice atoms can be replaced with an element with a different amount of valence electrons, in a process called doping. If the dopant atom has one more/less valence electron than the average in the lattice, it is called an electron donor/acceptor, and donates one electron into the conduction band/captures one electron from the valence band. The result is one static charge at the position of the atom and one opposite mobile charge carrier in the lattice. Adding an electron to the conduction band this way is called n-type doping (because Negative charges are mobile in this case), while adding holes to the valence band is known as p-type doping. The more dopants are added, the more mobile charges are present in the semiconductor. If the doping level is high enough, semiconductors can even behave like metallic conductors.

2.1.3 p-n junctions

When part of a material is doped n-type and another p-type, at the intersection between the 2 doping regimes, the holes from the p-doped part recombine with the electrons from the n-type part. Such a region between doping regimes is called a p-n junction[10]. Due to diffusion, charge carriers will flow in the direction of the oppositely doped region, while they are repelled by the electric field that is formed by the immobile dopant atoms that are left behind once the charge carriers have recombined (Figure 2.3). An equilibrium between drift and diffusion currents is thus present in the junction. The region around the p-n junction where charges have recombined is called the depletion region or space charge region. When a forward bias is applied to a p-n junction (i.e the n-type part of the material is connected to the negative side of a voltage source), electrons are injected into the n-type doped part while holes are injected into the p-type doped part. These excess carriers can than

flow through their respectively doped regions towards the junction, where they recombine, potentially emitting light by radiative recombination.

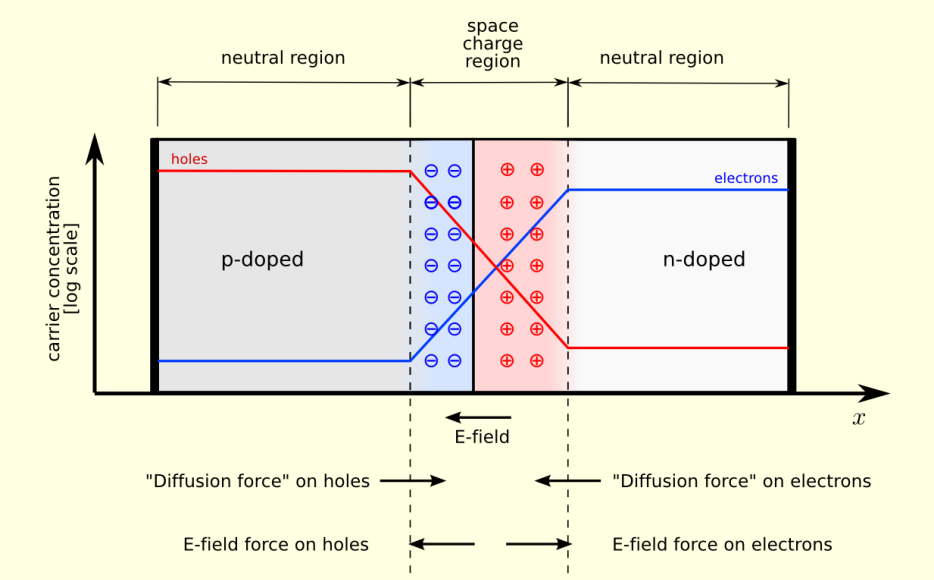

Figure 2.3. A schematic of a p-n junction in a semiconductor. At the interface between an n- and p-type doping regime, holes and electrons recombine, leaving behind charged dopant atoms, which results in an internal electric field. The space charge region is the result of an equilibrium between drift and diffusion currents[11].

2.1.4 Metal-semiconductor contacts

The type of contact that is formed between a semiconductor and a metal depends on the Fermi level in the semiconductor and the work function of the metal. The Fermi level is equal to the energy level of the (imaginary) state that has a 50% chance of being occupied by an electron in thermal equilibrium. In intrinsic silicon, the Fermi level lies exactly in the middle between conduction and valence band; n-type doping raises the Fermi level closer to the conduction band while p-type doping has the opposite effect. If the Fermi level of the semiconductor is higher than that of the metal with which it is contacted, electrons can lose some free energy by flowing into the metal, similar to what happens in a p-n junction. Due to the charged dopants that are left behind as the electrons flow into the metal, an electric field develops which stops more charge from flowing in. This electrical field, again akin to the p-n junction, stops electrons from flowing and a so-called Schottky barrier is formed (Figure 2.4). Due to the charges that are present near the metal-semiconductor interface the electrons experience a different electrostatic potential depending their position relative to the interface, which is reflected in bending of the vacuum, conduction band and valence band energy levels.

If the Fermi level in the semiconductor is lower or about equal to that in the metal, electrons flow into the semiconductor or barely move at all, and a metallic contact is formed, that allows electrons to freely enter and exit the semiconductor. For holes however, the opposite holds true; they will cross over most easily when the Fermi level in the semiconductor is higher than that of the metal. To obtain high currents in semiconductors, it is thus important to choose suitable contact materials, that allow movement of carriers across the metal-semiconductor interface.

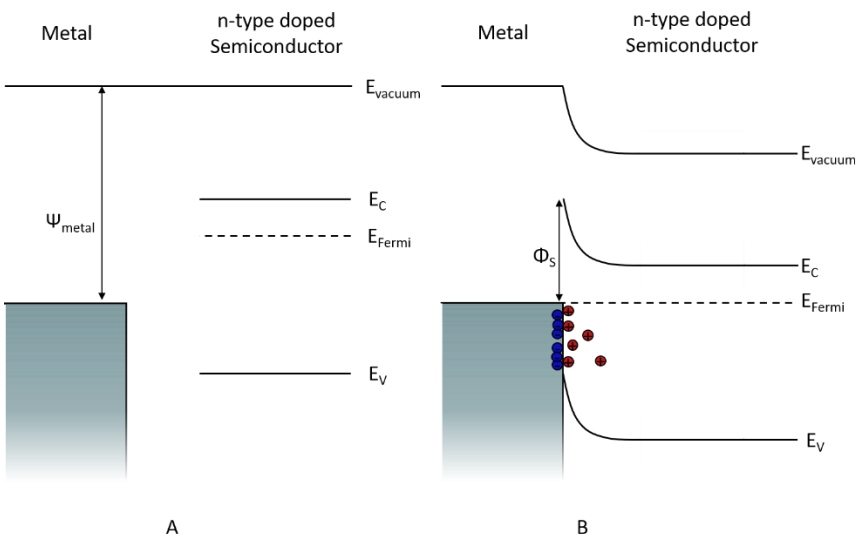

Figure 2.4. Schematic of a Schottky contact. A) The energy levels vs. vacuum in the metal and semiconductor before contact. The Fermi level in the semiconductor is closer to the conduction band than the valence band due to the n-type doping. B) The energy levels after contact between the two materials. Electrons have flowed to the lower energy level in the metal, leaving positively charged dopants behind. Chemical equilibrium is reached once the Fermi level in the semiconductor is equal to HOMO in the metal. Φ_S is the Schottky barrier energy.

2.2 colloidal quantum dots

Bulk III-V and II-VI semiconductors feature well-defined conduction and valence bands, and a material-dependent band gap. In nanoparticles form the same materials however, the band gap no longer is a material property, but depends instead on the size and shape of the particle. Electrons are confined to the dimensions of smaller crystals. Similar to the electron-in-a-box model, the more confined the electrons are, the larger the energy difference between states, and thus the larger the bandgap in a nanocrystal. When considering the LCAO model less atomic orbitals are available in smaller crystals, which leads to less states with a larger energy difference between them. The overall decrease in density of states in nanocrystals also results in less well-defined bands. Especially near the band gap edges, the energy difference between 2 states can become large enough that separate transitions can be distinguished (Figure 2.5).

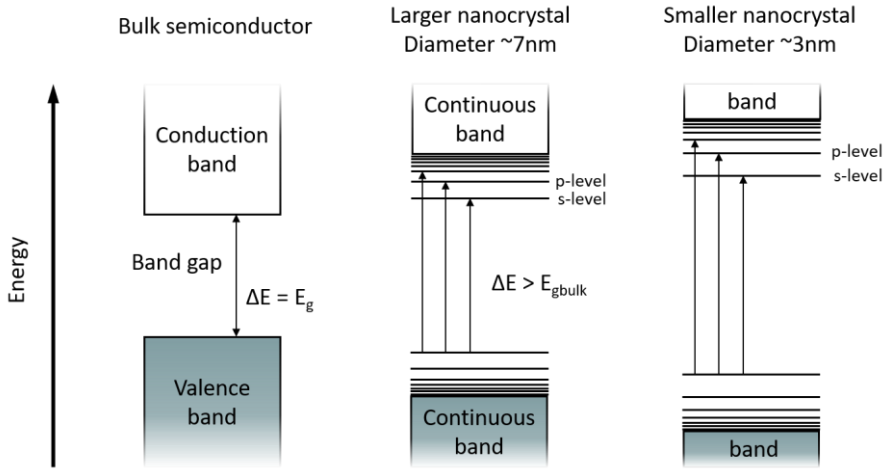

Figure 2.5. The band structure of both bulk and nanocrystal semiconductors. Due to quantum confinement, the bandgap increases with smaller nanocrystal size and the energy difference between levels near the bandgap also increases with smaller crystal size.

The size-tunable band gap of semiconductor nanocrystals has attracted a lot of attention, as it is usually quite difficult to finetune or even modify the band gap of a certain material. However, nanocrystals are inherently unstable due to the large amount of surface states. To protect the surface and ensure the electrons are really confined inside the particle, molecules known as ligands can be bound to the surface atoms of a nanocrystal. When an apolar organic ligand is used, it can both pacify the surface and allow dissolution of the nanoparticles in organic solvents like hexane, greatly improving the processing options. Nanoparticles dissolved this way are often called colloidal quantum dots (QDs). However, the surface atoms of the ligated QDs can still have some dangling orbitals that can introduce strap states. These trap states can have energy levels in the band gap resulting in non-radiative recombination and a lower photoluminescence quantum yield. To improve the low photoluminescence quantum yield, the ligand layer can be optimized, or a shell layer can be grown around the dot using a different material. Shell growth mostly passivates the surface states and leads to a drastically higher quantum yield[12]. By growing a CdS shell around CdSe quantum dots, near-unity photoluminescence quantum yields can be obtained, indicating most of the trap states have been pacified[4].

Because they are much more sensitive to disturbances in the lattice and the surface specifically, impurity doping of QDs has been a major challenge. Introducing a dopant adds extra states to the system, which can act as traps for carriers, impeding radiative recombination or conductivity[7]. Additionally, the added electrons or holes can make the quantum dot even more reactive, which can rapidly lead to degradation of the quantum dots[8]. Therefore, there have been attempts to introduce excess carriers in other ways than lattice doping, among which redox injection, where additional electrons are transferred from other compounds into the QDs in a redox reaction[13, 14] and

photodoping, where the electron is optically excited and the hole then transferred to another compound[15, 16]. Another method to introduce holes or electrons is electrochemical doping[9]. When colloidal quantum dots are loaded into an electrochemical cell along with an electrolyte and a voltage is then applied to the working electrode connected to the QDs, the Fermi level of carriers in the positive/negative electrode drops/rises compared to the valence/conduction band, and holes/electrons are injected into the material. This injection of carriers into the quantum dots is accompanied by a movement of the dissolved ions to achieve local charge neutrality as much as possible (Figure 2.6). This way, a temporary doping is achieved. However, when the voltage is turned off, the system relaxes to its intrinsic state.

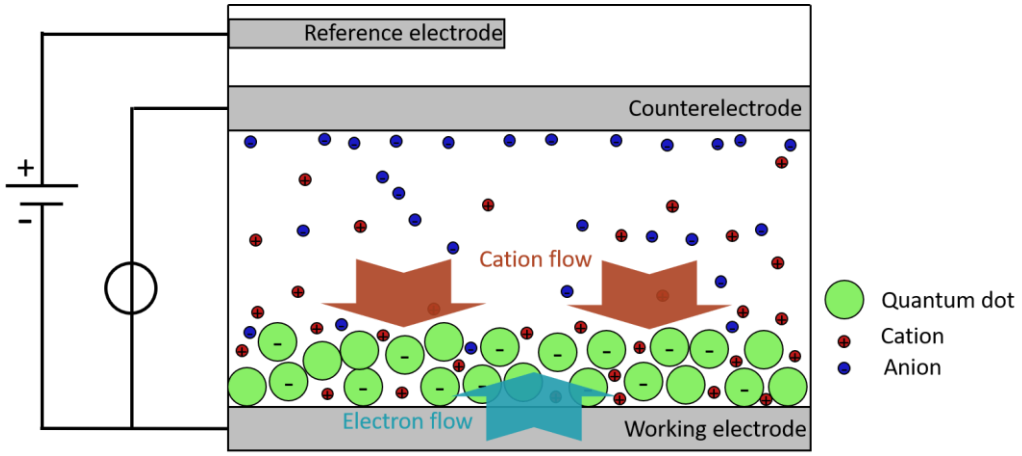

Figure 2.6. Electrochemical doping of colloidal quantum dots. When a voltage is applied to the cell, charge carriers are injected into the quantum dots, while charge neutrality is preserved by a flow of oppositely charged ions.

Although the conductivity in quantum dot films can be increased by doping, it remains lower than in bulk semiconductors[17, 18], because charge carriers have to tunnel from dot to dot in order to be mobile in QD films, instead of simply moving through the lattice. The tunnelling probability depends strongly on the coupling between the dots, and thus on the interdot distance[19]. The packing density of quantum dots can be increased by e.g. binding shorter ligands to the surface[20, 21], crosslinking ligands[22] or using different deposition techniques[23, 24].

2.3 Light-emitting electrochemical cells

When a porous semiconductor is mixed with an electrolyte, a system is created which contains mobile electrons, holes and ions. If this system is sandwiched between two electrodes and a voltage is applied, electrochemical doping can take place on both sides of the semiconductor material. Cations move towards the negative electrode, where electrons are injected, while anions move towards the positive electrode where holes are injected. When this process is completed, a part of the material is p-doped and the other n-doped, effectively creating a dynamic p-n junction in between the two regimes. As long as the voltage is applied to this system, electrons and holes enter on opposite sides, flow towards the junction through the doped regions and recombine in the middle to emit light. Such a system is called a light-emitting electrochemical cell (LEC), as first described by Pei *et al*. in 1995[1]. Their LEC was based on the semiconducting polymer poly[2-methoxy-5-(2-ethylhexyloxy)-1,4-phenylenevinylene] (MEH-PPV) mixed with the solid electrolyte poly(ethylene oxide) (PEO) and lithium trifluoromethanesulfonate ($LiCF_3SO_3$) to provide the mobile ions. The device is completely solid, and the mixture of compounds can be spincast as a single layer on top of which electrodes can be deposited. This easy processing is one of the most promising upsides of LECs. One year after the first

publication, LECs based on Ru-complexes (called ionic transition metal complex- or iTMC-LEC) were developed by Maness *et al.*[25]. Although the materials used in these devices are quite different, the working principle is similar.

Attempts have also been made to produce quantum dot-based LECs. Norell Bader *et al.* combined a semiconducting polymer (PF/PPV) with CdSe quantum dots[26]. The device operated as a normal polymer LEC, except that instead of recombining in the polymer, the charges were transferred to the quantum dots were they then recombined radiatively. Because the polymer handles all the charge transport, the poor conductivity of quantum dots is effectively bypassed. This device showed bright and narrow emission, but the turn-on voltage was very high (~7V) and the maximum efficiency was only 0.1%. Another group achieved full white-light emission from QD-based LECs with low turn-on voltages (2V for the red-emitting dots)[27]. Here, CdSe quantum dots ligated with 4-mercaptobenzoic acid (4-MBA) were used in the active layer together with polyvinylcarbazole (PVK) as hole-conducting polymer and the ionic liquid BMIM-PF_6. LECs with 4 different sizes quantum dots were made, resulting in different emission spectra: red, orange, green and blue. A white LEC was also made by adding different sizes quantum dots together. In the device of Qian *et al.*, PVK is used as a hole transporting species, so it may be possible that the quantum dots were not actually p-doped, but instead the holes were injected into it by the PVK while electrons were transported through the dots.

Before 2010, two models were proposed to explain the potential profile in a polymer-based LEC: the electrodynamical (ED)[28] and electrochemical doping (ECD)[29] model (Figure 2.7). The ED model predicts the formation of a large electric double layers (EDLs) near the electrode, where a lot of ions accumulate. This results in a region without an electric field throughout most of the device, which means carrier transport is diffusion-limited. Both positive and negative ions can be found anywhere in the field free region. Although recombination and light emission can take place, the light emission intensity is limited by the low diffusion current density. In the ECD model, a smaller EDL is formed, only enough to form an Ohmic contact between the electrode and the semiconductor. The rest of the ions have migrated to their respective half of the material, resulting in a n- and p-doped region and only a thin junction in the middle, where recombination and luminescence take place. In the doped regions, carrier concentrations are relatively high, allowing larger current densities compared to the ED profile. Since the concentration of both cations and anions in the space charge region is zero, technically, a p-i-n junction (i for intrinsic) is formed, in contrast to inorganic semiconductor LEDs where ionized dopants are still present in the space charge region. This type of junction works very similar to a normal p-n junction. However, the electric field in the p-i-n junction exists due to the unpaired electrons and holes instead of ionized dopants.

In 2010, a unifying model was proposed by van Reenen *et al.*[30]. In this model the developed electrostatic profile depends on the injection of carriers from the electrodes into the LEC material. If the injection barriers (defined as the amount of energy needed for a charge carrier to move from the electrode into their respective band) are high compared to the applied bias, carrier injection is limited, and an ED profile develops. If the injection barriers however are small compared to the applied bias, a p-i-n junction may be formed, which is favourable for the recombination and thus luminescent properties of the LEC.

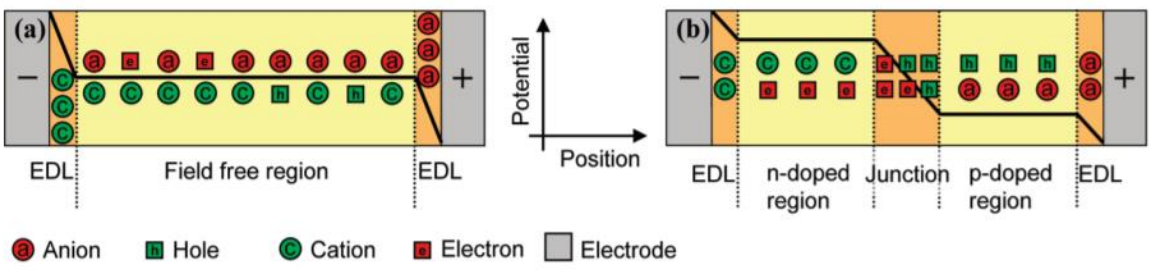

Figure 2.7. A) Prediction for potential profile based on the ED and B) ECD model. In the ED model, the predicted current density and recombination intensity is lower than in the ECD model[30].

Compared to LEDs, LECs have long turn-on times. Because the movement of ions is necessary for operation, it takes at best a few seconds before the device starts emitting light after a voltage is applied. Although for ambient lighting this is not an issue, for application in screens, where refresh rates below 16 ms are required, dynamic junction LECs are not an option. Once the LEC is turned on, the junction is stable for as long as the voltage is held, but as soon as the voltage is released, the system relaxes and ions diffuse back while charges flow out of the device. There have been attempts to immobilize the ions after charging the device[31-33]. If ions can be fully immobilized though this so-called charge fixing, charge carriers are kept in the device due to electrostatic forces and the p-n junction would be preserved even when the bias is turned off. Ionic liquids or polymerizable salts can be used for this purpose. After applying a sufficient voltage and forming the junction, electrochemical doping can be fixed either by reducing the temperature (“freezing”) or polymerising the electrolyte.

Experimental

All materials that were used are listed in section 3.1. In sections 3.2 and 3.3, ZnO and CdSe/CdS/ZnS quantum dot synthesis is described. Section 3.4 contains the ligand exchange procedure of the CdSe/CdS/ZnS QDs. The ligand exchange was analysed by FTIR as described in section 3.5. In section 3.6 it is explained how the LEC devices were produced. The setup and details of (spectro)electrochemical analysis of these devices is described in sections 3.7 and 3.8. Finally, in section 3.9, all details, starting conditions and equations used in the computational simulations are discussed. It is also explained how the model is operated.

3.1 Materials

The following materials were used as received: zinc acetate dihydrate ($Zn(CH3COO)_2{\cdot}2H_2O$ reagent grade, Sigma-Aldrich), zinc acetate (Sigma-Aldrich, 99.99%, <0.2% H_2O), potassium hydroxide (KOH pellets, Sigma-Aldrich), cadmium acetate (Chempur, 99.999%), trioctylphosphine oxide (TOPO, Sigma-Aldrich, 99%), trioctylphosphine (TOP, Sigma-Aldrich, 97%), octadecylamine (ODA, Sigma-Aldrich, 97%), anhydrous methanol (VWR International BV, 99.9%), anhydrous ethanol (Sigma-Aldrich), anhydrous butanol (Sigma-Aldrich, 99.8%), anhydrous methyl acetate (Sigma-Aldrich, 99.5%) anhydrous toluene (Thermo Fisher, 99.8%), anhydrous chloroform (Sigma-Aldrich, 99%), 1-octanethiol (Sigma-Aldrich, 98.5%), pivalic acid (PA, Sigma-Aldrich, 99%), trimethylamine (Sigma-Aldrich, 99.5%) and 1,2-dichlorobenzene (Sigma-Aldrich, 99%). The solids poly[2-methoxy-5-(2-ethylhexyloxy)-1,4-phenylenevinylene] (MEH-PPV, Sigma-Aldrich, M_n = 40,000-70,000), poly(ethylene oxide) (Sigma-Aldrich, average M_v ~5,000,000), lithium trifluoromethanesulfonate ($LiCF_3SO_3$, Sigma-Aldrich, 99.99%) and selenium (Sigma-Aldrich, 99.99%) were degassed by keeping them under vacuum overnight for at least 16 hours. The liquids oleic acid (OA, Sigma-Aldrich, 90%), octadecene (ODE, Sigma-Aldrich, 90%), oleylamine (OLAM, Sigma-Aldrich, 70%) and cyclohexanone (Sigma-Aldrich, 99.8%) were degassed by heating *in vacuo* until bubble formation was no longer observed in the liquid. All procedures were executed in an inert nitrogen atmosphere ($[O_2]$ < 30 ppm, $[H_2O]$ < 1 ppm) unless otherwise stated.

3.2 ZnO QD synthesis

The synthesis of zinc oxide nanocrystals (NCs) was performed as described by Gudjonsdottir et al.[34]. Typically, 3.425 mmol of zinc acetate dihydrate and 50 mL of ethanol were added to a flask and heated to 60 °C. In a separate flask, 6.25 mmol of KOH and 5 mL of methanol were combined and stirred at room temperature. When both reagents had dissolved, the potassium hydroxide mixture was dropwise added to the stirred zinc acetate dihydrate mixture. The solution was stirred for 1 min more before the heat source was removed. The QDs were purified by adding hexane until the solution became turbid. The flocculates were isolated by centrifugation at 2000 rpm for 1 min and redissolved in ethanol. The QD dispersion was stored at −20 °C to avoid further growth by Ostwald ripening.

3.3 CdSe/CdS/ZnS QD synthesis

The synthesis of the CdSe/CdS/ZnS QD was done following a hot injection procedure of Qu et al[35].

CdSe core synthesis. 0.66 g cadmium acetate, 3.68 g OA and 25.9 g ODE was added to a 3-neck round-bottom flask. This mixture was degassed *in vacuo* under constant stirring for 3 hours at 120 °C, after which the cadmium precursor (cadmium oleate in ODE) was obtained. The cadmium precursor was melted at 60 °C before use. The selenium precursor was prepared by mixing 1.42 g selenium, 7.5 g TOP and 11.9 g ODE in a 50 mL vial. This mixture was stirred at 80 °C until the selenium was fully dissolved. 3.2 g ODA and 1.11 g TOPO was added to a 3-neck round-bottom flask under normal atmosphere. The flask was connected to a Schlenk line and put under nitrogen atmosphere. Under constant stirring, the

temperature was raised to 150 °C so that the solids melted to form a colourless liquid, which was degassed *in vacuo* for 1 hour. Then 5.2 g of the selenium precursor was added and the temperature was raised. As soon as the mixture reached 300 °C, 4.9 g of the Cd-precursor was injected as quickly as possible using 2 syringes. The temperature was lowered to 280° C and the NCs were grown for 4 minutes. The flask was then cooled with an air gun, and once the temperature reached 50 °C, 5 mL anhydrous toluene was added to fully quench the reaction (Figure 3.1). The mixture was extracted by syringe and divided over four 50 mL vials for washing. To each vial, 8 mL anhydrous methyl acetate and 3 mL anhydrous methanol was added to flocculate the QDs, after which they were centrifuged for 8 minutes at 3500 rpm. The supernatant was removed and 5 mL methylacetate and 3 mL methanol was added to each vial, after which the QDs were again centrifuged for 8 minutes at 3500 rpm. The supernatant was removed and the dots were combined and dissolved in 13 mL anhydrous toluene, yielding the transparent dark-red CdSe quantum dot solution.

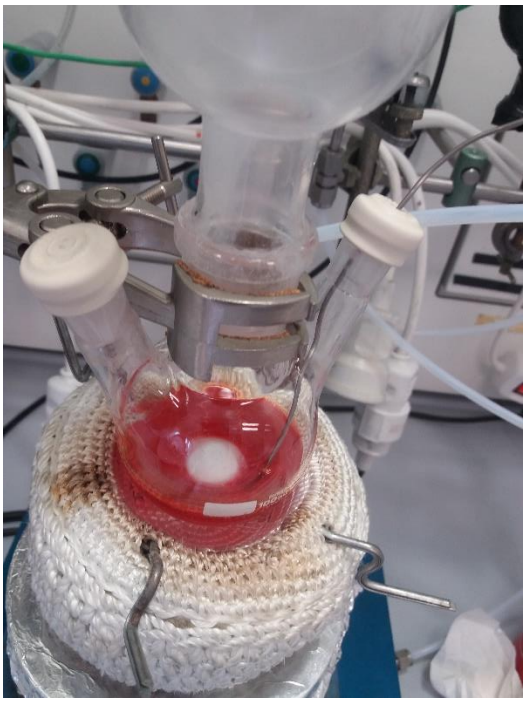

Figure 3.1. The CdSe QD dispersion in the 3-neck round-bottom flask. This picture was taken right after quenching the growth reaction.

CdS and ZnS shell addition. To make the zinc precursor, 0.354 g OA was added to 0.059 g zinc acetate. This mixture was stirred for 2 hours at 130 °C to obtain zinc oleate and evaporate the acetic acid that was produced as a side product. Then 170 µL oleyamine (OLAM) and 3.5 mL ODE was added to the mixture. Before use, the precursor was heated to 90 °C under constant stirring to fully dissolve the zinc oleate. 0.82 mL of the CdSe core quantum dot solution and 1.5 mL ODE was added to a 3-neck round-bottom flask. The temperature of this solution was raised to 310 °C under constant stirring. Starting when the temperature reached 240 °C 6 mL of the sulphur precursor (0.074 M octanethiol in ODE) and 6 mL of the cadmium precursor was added dropwise over 6 hours. The mixture was cooled down to room temperature and left overnight. The temperature of this mixture was raised again to 290 °C. Dropwise addition of the zinc and sulphur precursors started when the mixture reached 240 °C. 3 mL of zinc precursor and 3 mL of sulphur precursor was added over 3 hours. The mixture was then cooled to room temperature using compressed air, extracted by syringe and divided over 4 vials. To each vial 8 mL of anhydrous methyl acetate and 3 mL anhydrous methanol was added, and the vials were centrifuged for 8 minutes at 3500 rpm. The supernatant was removed and the nanoparticles were combined and redissolved in 12 mL anhydrous toluene, yielding a transparent, dark-red solution.

3.4 CdSe/CdS/ZnS QD ligand exchange

The ligand exchange procedure was adapted from a method designed for CdSe core QD[36]. The concentration of the CdSe/CdS/ZnS quantum dot solution was determined to be 60 mg/mL by drying and weighing the residue of 100 µL of the solution. A pivalic acid (PA) stock solution was made consisting of tri-ethylamine, PA (after melting at 60 °C), and 1,2-dichlorobenzene mixed in volume ratio 2:3:4. Then 1.2 mL (containing 72mg QD) of the CdSe/CdS/ZnS solution and 2 mL of the PA stock solution were mixed and left in the dark for one hour. 4 mL of anhydrous methanol was added to flocculate the QD, and they were centrifuged for 5 minutes at 3000 rpm. The supernatant was discarded and the residue redissolved in 2 mL of the stock solution. Flocculation, centrifugation and redispersion were repeated 3 more times in the same way except using only 2 mL of methanol. The last time the QD were redissolved in 2 mL anhydrous chloroform. The appearance of the quantum dot solution had not changed after the ligand exchange. FTIR spectra were obtained of the QD both before and after the ligand exchange procedure, as well as all the ligands and solvents that were used in the preparation and exchange procedure.

3.5 ATR FTIR

100 µL of the QDs as obtained from the synthesis was dried *in vacuo* and redispersed in chloroform. ATR FTIR spectra were taken of this solution, the QD dispersion after ligand exchange in chloroform, PA, the possible native ligands TOP, TOPO, OA, oleyamine, some solvents used in the ligand exchange chloroform and triethylamine, and zinc acetate as a reference for the deprotonated organic acid group. All spectra were measured in absorbance in the range 4000-700 cm^{-1}.

3.6 Preparation of LEC devices

Polymer LECs based on MEH-PPV. The procedure used to produce the polymer LECs was adapted from the one reported by Li et al.[37]. A solution of poly[2-methoxy-5-(2-ethylhexyloxy)-1,4-phenylenevinylene] (MEH-PPV) in anhydrous chloroform (10 mg/mL) was made, as well as solutions of poly(ethylene oxide) (PEO) and lithium trifluoromethanesulfonate ($LiCF_3SO_3$) in cyclohexanone (both 10 mg/mL). These 3 solutions were mixed together in volume ratio 12:5:2 MEH-PPV:PEO:$LiCF_3SO_3$ to make the master solution used for spin coating. This master solution was stirred at 50 °C for at least 30 minutes before use. Glass substrates covered with indium tin oxide (ITO) (thickness ~ 100 nm) were placed in a petri dish containing a layer of aqua regia (HCL:HNO_3 3:1), so that they were half submerged. The substrates were left for 5 minutes as the ITO was fully etched from the submerged part rendering it non-conductive. On top of these substrates, the LEC films were prepared by spin coating about 100 µL of the master solution at 2000 rpm for 120 s, followed by 4000 rpm for 60 s. The substrates were dried for at least 2 hours at 50 °C to evaporate any remaining solvents from the film. As the opposite electrode, 200 nm of aluminium was then deposited under high vacuum (10^{-6} mbar) in a stripe pattern, so that aluminium electrodes overlaid both halves of the substrate (Figure 3.2). These devices could be clamped on the bottom side to connect them to the potentiostat while leaving the top available for optical measurements.

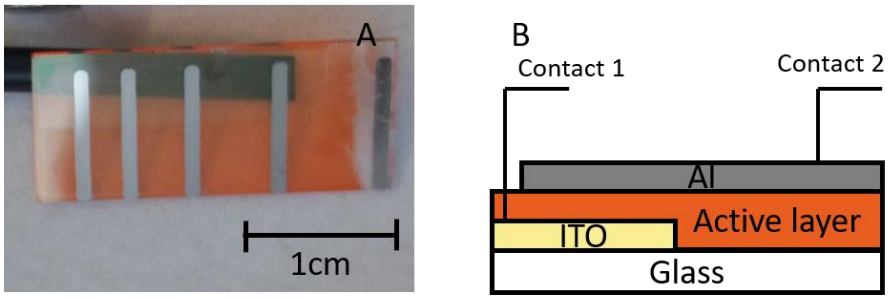

Figure 3.2. The MEH-PPV based LEC. A) Top view of the device . The ITO layer has been etched from the bottom half, as can be seen by a slight difference in the colour of the substrate. B) Schematic cross-sectional view of the device architecture. The same design was used for the quantum dot LECs.

Quantum dot LECs based on CdSe/CdS/ZnS. The CdSe/CdS/ZnS quantum dot master solution was made by mixing 0.317 mL of the ligand exchanged CdSe/CdS/ZnS in anhydrous chloroform (63mg/mL), 1.638 mL chloroform, 0.5 mL PEO in cyclohexanone (10 mg/mL) and 0.1 mL $LiCF_3SO_3$ in cyclohexanone to obtain a mixture with a concentration of 10 mg/mL and a mass ratio of 20:5:1 (QD:PEO:$LiCF_3SO_3$). This mixture had a yellow-orange colour but still showed bright red photoluminescence. The quantum dot master solution was stirred at 50 °C for 30 minutes before use. On a half-etched ITO substrate, 100 µL of the quantum dot master solution was drop cast and carefully blown dry using an air gun (Figure 3.3 A). Another sample was spin coated by depositing 4 consecutive layers of 100 µL on a half-covered ITO substrate and spinning at 800 rpm for 60 seconds after each deposition. The drop casted sample showed a much thicker active layer (Figure 3.3 B). Both samples were dried at 50 °C for 45 minutes, and 200 nm of aluminium was deposited under high vacuum (10^{-6} mbar) in a stripe pattern.

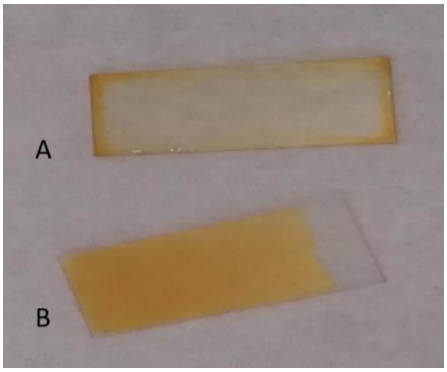

Figure 3.3. Spin coated (A) and drop cast (B) quantum dot/PEO layers. The drop cast film is thicker than the spin coated one, which helps to prevent pinholes in the device.

Quantum dot LECs based on ZnO. As zinc oxide is fully air-stable, ZnO films were produced in ambient conditions. The concentration of the ZnO dispersion was determined to be 12.58 mg/mL by drying 200 µL of the solution and weighing the residue. To 0.795 mL of the ZnO dispersion, 205 mL of ethanol, 0.250 mL of PEO in ethanol (10 mg/mL) and 0.050 mL of $LiCF_3SO_3$ in ethanol (10 mg/mL) was added to obtain the ZnO master solution with a concentration of 10 mg/mL and a mass ratio of 20:5:1 QD:PEO:$LiCF_3SO_3$. A control solution without $LiCF_3SO_3$ was also prepared. Both solutions were refrigerated at -20 °C immediately after creation. On top of half-etched ITO substrates, 120 µL of the ZnO master solution or ZnO control solution was deposited and left undisturbed until the solvent had evaporated. Two more layers were added on top in the same way but were blown dry carefully with an air gun without causing flow in the liquid. Both films were colourless and opaque but homogeneous. Both samples were dried at 50 °C for 45 minutes, and 200 nm of aluminium was deposited under high vacuum (10^{-6} mbar) in a stripe pattern.

3.7 Cyclic voltammetry measurements

The LEC devices were clamped and contacted by loading them in a special cap as shown in Figure 3.4. The devices were connected to a PGSTAT128N Autolab potentiostat, which was used to perform voltammetry cycles and voltammetric linear sweeps at a scan rate of 0.01 V/s.

3.8 Spectroscopy measurements

While clamped in the cap, photoluminescence of the film was measured by probing the sample with a 405 nm Thorlabs laser under a 45° angle. The emitted light was focussed with a lens onto a fiber-based Ocean Optics USB2000 UV-vis spectrometer. Transient electroluminescence was measured by performing a cyclic voltammetry measurement while constantly taking the electroluminescence spectrum.

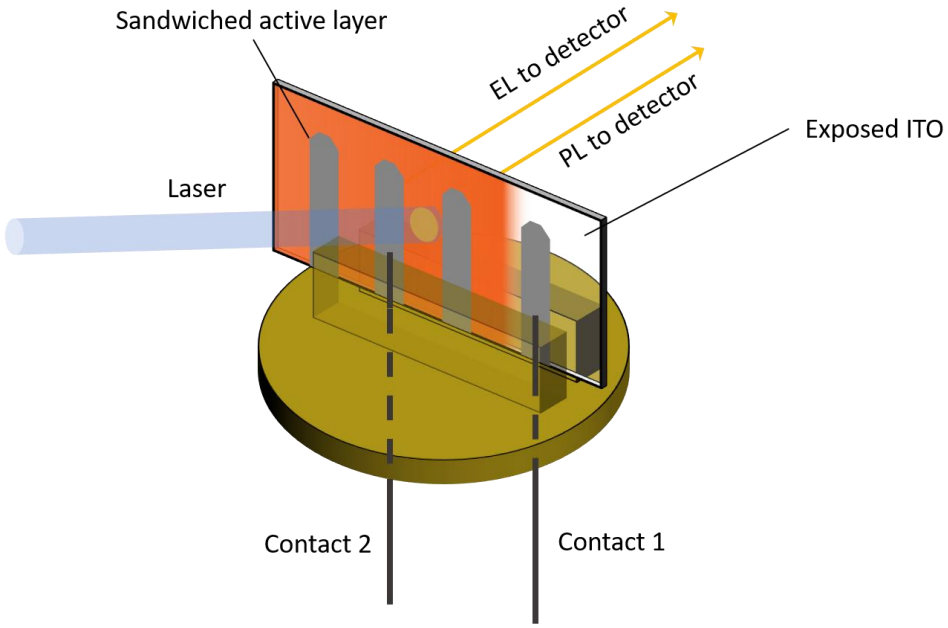

Figure 3.4. The setup used to measure photoluminescence and (transient) electroluminescence. To connect the sample to the potentiostat, the Al-coated front side of the sample is pressed into the metal contacts from behind, while light can freely be emitted from the top side to be collected by the detector. The top side is also available for a laser beam and a white light beam to take photoluminescence and absorption measurements of the film.

3.9 Computational details

A 1-dimensional model was used based on the LEC model by van Reenen et al.[30]. The space between the two electrodes was divided in grid points, and for every point the concentration of 4 types of charge carriers was defined: electrons, holes, anions and cations. Initially all carriers are homogeneously distributed throughout the device; cation and anion concentrations are both equal to the given starting value while electrons and hole are present at their intrinsic concentrations. It is assumed that the electric field F is constant before any carrier movement has taken place, i.e. the electrostatic potential V drops linearly over the device. The transient simulation is then started by taking small time steps. Each step the following procedure is executed:

1. Holes and electrons are injected into the semiconductor from the electrodes according to a modified Boltzmann injection model.

2. The electric field and electrostatic potential versus distance are calculated by solving the Poisson equation for the given boundary conditions.
3. Using drift-diffusion equations, the current densities in between all grid points are calculated separately for each charge carrier.
4. The recombination of electrons and holes is calculated for each grid point.
5. The concentrations of the charge carriers are updated using the continuity equations.

The simulation is run until steady state is reached, i.e. when the current density of both ions becomes zero everywhere in the device. Each step together with the associated equations and assumptions will be discussed in detail below.

Step 1: electron and hole injection. To efficiently model the movement of charges from the electrodes into the semiconductor, a lot of simplifications must be made. The electron and hole concentrations in any semiconductor can be calculated using the Boltzmann approximation:

$$\boldsymbol{n = N_C * \exp\left(\frac{-(E_C - E_F)}{kT}\right)} \quad \textbf{(3.1)}$$

$$p = N_V * \exp\left(\frac{-(E_F - E_V)}{kT}\right) \quad \textbf{(3.2)}$$

Where n and p are the electron and hole concentrations, N_C and N_V are the effective density of states in the conduction and valence band and E_C, E_V and E_F are the conduction band, valence band, and Fermi energy levels. In the model an instant equilibrium of charge carriers between the metal contact and the edge of the interface is assumed, i.e. the Fermi level is constant over the interface of the materials. The electron and hole concentrations at the outermost grid points can thus be calculated using equation 3.1 and 3.2 while substituting E_F for the Fermi level inside the electrodes.

Step 2: Calculating the electric field and electrostatic potential. The second space derivative of the electrostatic potential (V) is determined only by charge distribution and can be calculated in every grid point using the one-dimensional Poisson equation:

$$\boldsymbol{\frac{d^2V}{dx^2} = -\frac{q}{\varepsilon_r \varepsilon_0}(p - n + c - a)} \quad (3.3)$$

Where p, n, c and a are the concentrations of holes, electrons, cations and anions, respectively. The electric field and electrostatic potential can then consecutively be calculated by solving the differential equations with the following boundary conditions:

$$\int_0^L F dx = V_{bias}$$

$$V_{positive\ electrode} = V_{bias}$$

Where V_{bias} is the applied bias, F is the electric field and L is the thickness of the device. Consequently, V is always equal to zero at the negative electrode.

Step 3: Calculating current densities. The current densities across the device are calculated using drift-diffusion equations:

$$\boldsymbol{J_n = qn\mu_n \frac{dV}{dx} + kT\mu_n \frac{dn}{dx}} \quad \textbf{(3.4)}$$

$$J_p = qp\mu_p \frac{dV}{dx} - kT\mu_p \frac{dp}{dx} \quad \textbf{(3.5)}$$

$$J_a = qa\mu_a \frac{dV}{dx} + kT\mu_a \frac{da}{dx} \quad \textbf{(3.6)}$$

$$J_c = qc\mu_c \frac{dV}{dx} - kT\mu_c \frac{dc}{dx} \quad \textbf{(3.7)}$$

Where *n*, *p*, *a*, *c* are the electron, hole, anion and cation concentration. J_i is the current density corresponding to carrier *i* and μ_i is the corresponding mobility. Since the metal contacts are considered non-conductive to ions, the ion currents at the boundaries are set to zero.

Step 4: Calculating recombination. Recombination in each grid point is calculated according to the following equation:

$$\boldsymbol{R = \frac{q(\mu_n + \mu_p)}{\varepsilon_r \varepsilon_0} np} \quad \textbf{(3.8)}$$

Where *R* is the recombination rate, *n* and *p* are the electron and hole concentration and μ_n and μ_p their respective mobilities. The model as of yet has no way to take trap states or Auger recombination into account, and as such is not able to calculate luminescence efficiencies. Although some information regarding recombination can be obtained from the model, these data can only be compared qualitatively and for systems with similar starting conditions.

Step 5: Updating carrier concentrations. Lastly, the carrier concentrations are updated using the continuity equations:

$$\boldsymbol{\frac{dn}{dt} = \frac{1}{q}\frac{J_n}{dx} - R} \quad \textbf{(3.9)}$$

$$\frac{dp}{dt} = \frac{1}{q}\frac{J_p}{dx} - R \quad \textbf{(3.10)}$$

$$\frac{da}{dt} = \frac{1}{q}\frac{J_a}{dx} \quad \textbf{(3.11)}$$

$$\frac{dc}{dt} = \frac{1}{q}\frac{J_c}{dx} \quad \textbf{(3.12)}$$

Where *di* is the change in the concentration of carrier *i*, *Ji* is the corresponding current density as calculated in step 3, *R* is the recombination rate and *dt* is the size of the time step.

Standard LEC parameters. Some simulations were run with non-physical parameters to show what general trends and behaviours can be expected in LECs. These parameters were chosen to speed up convergence and reach steady state swiftly, and to make interpreting and understating the results as

straightforward as possible. A simple band structure was chosen with a LUMO, HOMO and Fermi level at -0.5, -1.5 and -1.0 eV versus vacuum, respectively. The work functions of both electrodes were chosen to be equal to the Fermi level in the semiconductor, resulting in a symmetrical device with injection barriers of 0.5 eV. The standard electron and hole mobility (μ_n and μ_p) were 10^{-6} $m^2V^{-1}s^{-1}$. This mobility was assumed to be independent of carrier concentration and electric field strength. High ion mobilities (μ_a and μ_c) of 10^{-7} $m^2V^{-1}s^{-1}$ were chosen, and the ion density was $1.25*10^{25}$ m^{-3}. The thickness of the device L was 350 nm, divided over 81 grid points, resulting in an interpoint distance of 4.375 nm. To make sure the device was fully symmetrical, the effective density of states $N_C = N_V = 3*10^{26}$ was equal for both the conduction and valence band. A relative dielectric constant $\varepsilon_r = 3$ was used. The temperature was always set to 300 K. A time step size $dt = 10^{-12}$ s was considered. It was checked that grid spacing and time step size did not affect the outcome of the simulation.

CdSe/CdS/ZnS quantum dot LEC parameters. Some simulations were intended to resemble a CdSe/CdS/ZnS quantum-dot based LEC. In this case, parameters were optimized for this specific system. A band structure was chosen based on values reported in literature[38]. A LUMO and HOMO of -4.4 and -6.5 eV versus vacuum were used, corresponding to QD with a bandgap of 2.1 eV. The Fermi level inside the semiconductor was assumed to be in the middle of the bandgap at -5.45 eV versus vacuum. For electrodes, work functions resembling ITO (-4.7), gold (-5.2) or aluminium (-4.5) were selected as these are the materials that were used in the experiments. The work function of aluminium was assumed to be just above the conduction band edge of the QD. In the model however, hole and electron injection are governed by Botlzmann equations (3.1 and 3.2), which require the Fermi level in the electrodes to be in between the band edges of the semiconductor, so a work function just below the conduction band edge was selected for aluminium to simulate a very low/non-existent injection barrier for electrons. This assured that electron injection was never limited. An electron mobility of $\mu_n = 1.5*10^{-10}$ $m^2V^{-1}s^{-1}$ was used[38], which was assumed independent of carrier concentration and electric field strength. Because hole conduction in CdSe QD is hard to achieve, no reported hole mobilities were found for CdSe quantum dot films, so a number of different mobilities were used in the simulations, all within an order of magnitude of the electron mobility. Similarly, the ion mobility in quantum dot/PEO films is unknown, but has been estimated for polymer-based LECs to be in the order of 10^{-10} $m^2V^{-1}s^{-1}$ at 360 K[39]. For the simulation at 300 K, a mobility of 10^{-11} $m^2V^{-1}s^{-1}$ was chosen for both cations and anions to roughly reflect the difference in temperature[40]. It should be noted that while the ion mobility is a critical parameter in real LECs, it does not affect the steady-state characteristics of the device. The ion density was estimated to be $3*10^{26}$ m^{-3} by assuming an average film density of 2 gcm^{-3} and the mass ratio mentioned above of 20:5:1 (QD:PEO:$LiCF_3SO_3$). Based on the same source that provided the band structure, an effective density of states $N_c = N_V = 3*10^{25}$ and a relative dielectric constant $\varepsilon_r = 4$ were chosen. The active layer had a thickness of $L = 200$ nm, divided over 99 grid points, resulting in an interpoint spacing $dx = 2.04$ nm. A time step size $dt = 10^{-8}$ s was used, reflecting the lower mobilities compared to the standard simulation. It was checked that the grid spacing and time step size did not affect the outcome of the simulation.

I-V curves. As a basis for the I-V curves, a system was simulated at $V_b = 0$ V. Once this system had reached steady state (recognised by a negligible change in electron current between time steps), the steady state current was recorded and the applied bias increased with 0.1 V, after which the simulation was run until steady state again. This process was repeated until $V_b = 4$ V. As a reference, an I-V curve was made using the standard parameters described above. For the CdSe/CdS/ZnS I-V curve ITO and aluminium were chosen as electrode materials, since these were the ones used in the experimental devices. To minimize computational time, electron and hole mobility were chosen to be equal at $1.5*10^{-10}$ $m^2V^{-1}s^{-1}$, while all other parameters were the same as described above for the CdSe/CdS/ZnS devices.

Experimental results and discussion

In this chapter the results are discussed that were obtained from the experimental devices. In section 4.1, the findings on optimizing the device architecture are presented. Section 4.2 deals with I-V behaviour and (transient) EL of polymer-based LECs. Then in section 4.3 the results of ZnO-based LECs are presented. Section 4.4 is about the ligand exchange of the CdSe/CdS/ZnS QDs, while in section 4.5 the I-V behaviour of these dots is discussed.

4.1 Device architecture

Two critical design requirements were identified for an LEC to be able to emit light that is visible to the naked eye. Firstly the distance between the two electrodes must be sufficiently small so that the ion migration and doping process can be completed in a few seconds. Secondly a sufficiently high shunt resistance is required to allow conduction through the active layer. The first requirement can be met by utilizing a sandwich-type structure (as opposed to a planar structure, see Figure 4.1 A) with an active layer thickness of about 200 nm[37]. However, a thin sandwiched active layer is very vulnerable and any physical contact may lead to a damage causing direct contact between the deposited aluminium electrode and the ITO, thereby short-circuiting the device (Figure 4.1 B). Since a metal needs to be pressed firmly onto the aluminium electrode to make an electrical contact, it is unlikely that the device can be connected to an instrument without punching through the active layer in the process. To prevent short-circuits, half of the ITO layer of a substrate was etched away before depositing the active layer (see section 3.4 for more details on device preparation), resulting in the device architecture as shown in Figure 4.1 C.

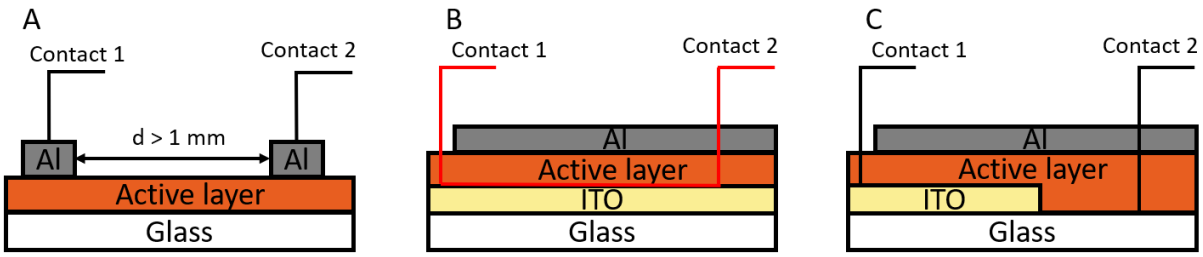

Figure 4.1. Different LEC device architectures. A) In a planar structure, the current through the device is low and the response is slow due to the larger interelectrode distance. B) In the sandwich structure, the metal contact can easily punch through the active layer, causing a short-circuit (shown in red). C) The device architecture used in electroluminescence experiments. Even if the metal contact punches through the active layer, it cannot touch the ITO.

4.2 LECs based on MEH-PPV

The I-V characteristic of a MEH-PPV LEC is shown in Figure 4.2. For small applied bias between roughly -2 and +2 V, the electrons and holes have insufficient energy to be injected into their respective bands. In this region, only a small ohmic current is observed due to pinholes, which is negligible compared to the currents at higher bias. When the bias is larger than the bandgap of the polymer, charge carriers are injected, and doping of the material is achieved. In this bias region, the maximum current density increases rapidly with applied bias as the doped regions are much more conductive than the intrinsic polymer.

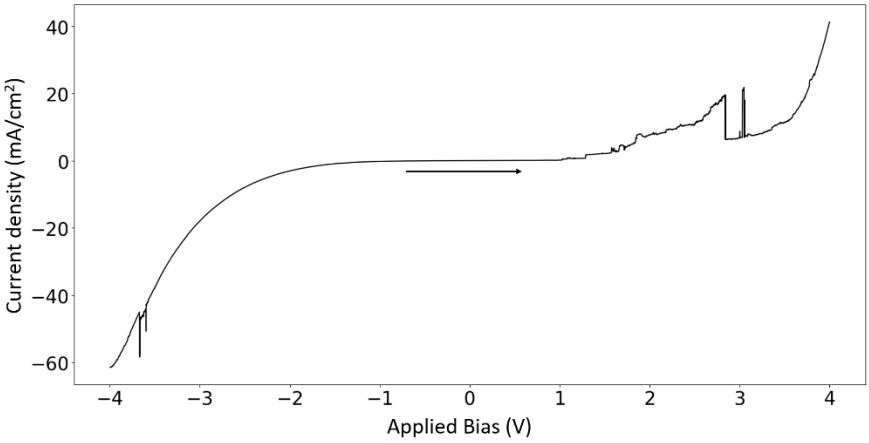

Figure 4.2. A typical I-V curve of a MEH-PPV based LEC. When the applied bias is between -2 and 2 V, very little current flows through the MEH-PPV as most charge carriers do not have enough energy to enter the bands of the semiconductor. When the applied bias is larger than the bandgap, doping occurs and the film becomes more conductive, leading to higher currents. Scan rate = 0.01 V/s, scan direction indicated by the arrow.

Apart from the noise, the I-V curve matches those found in earlier studies[41]. The symmetrical shape of the curve indicates fully reversible p and n-type doping as the junction is formed, relaxed and reformed with an opposite orientation in a single scan. Noise was always present in our I-V curves, independent of measurement device, scan speed or scan direction. This is most likely caused by defects in the film such as pinholes and heterogeneity of the film. Annealing the film may prevent these defects[37].

A cyclic voltammetry scan between 1.5 and 3 V is shown in the right panel of Figure 4.3 A. The qualitative light intensity determined by integrating the EL spectrum is plotted versus the applied bias in Figure 4.3 A left panel. The turn-on voltage of 2.3 to 2.4 V was determined by comparison between the onset and the end of the electroluminescence (Figure 4.3 B). This is in accordance with other values reported before[1, 32]. This value is slightly above the optical gap in MEH-PPV of 2.1 eV[42], possibly due to some additional resistances at the semiconductor-electrode interfaces which increase the injection barrier for holes or electrons.

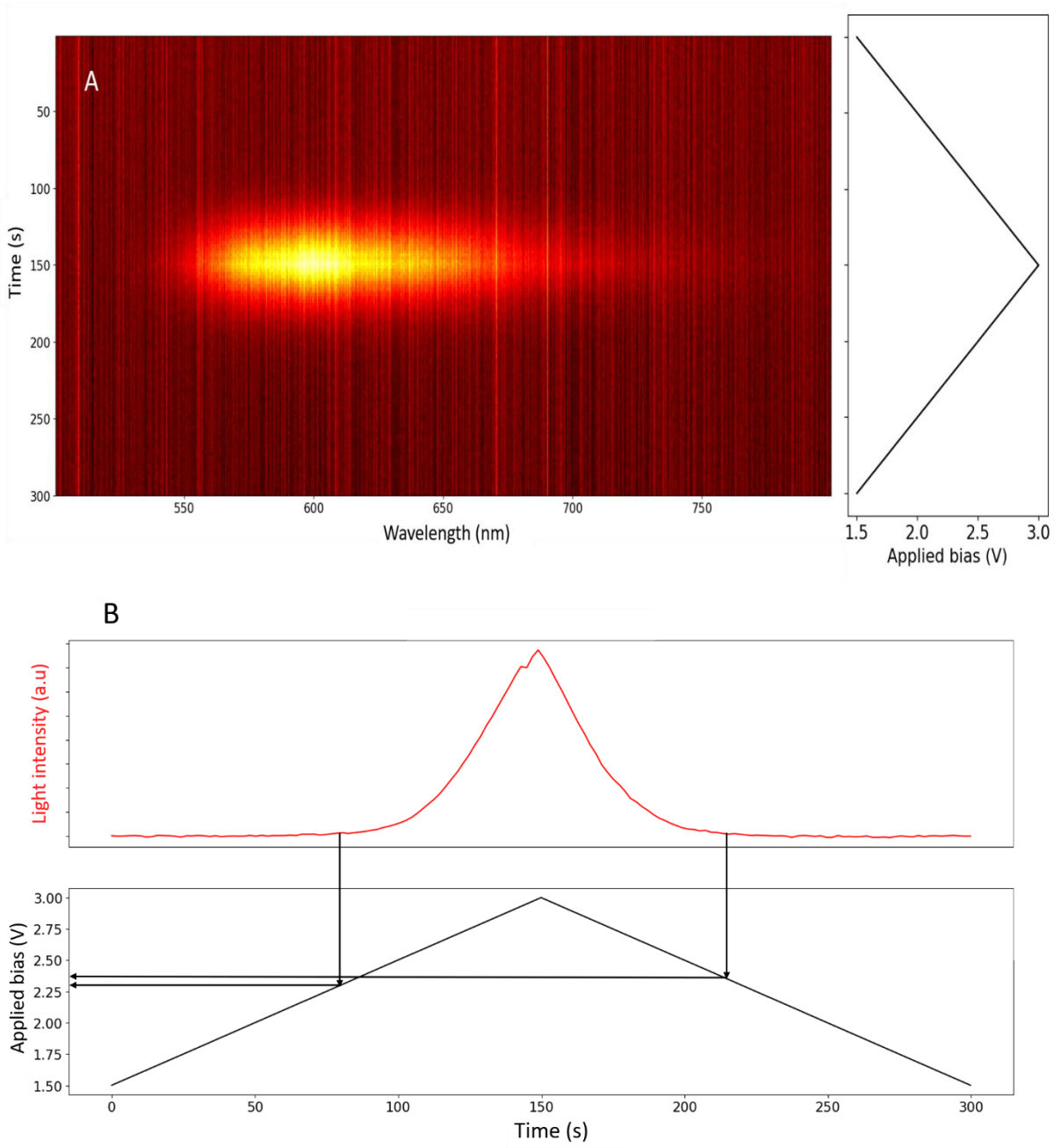

Figure 4.3. Light emission in a cyclic voltammetry scan with the voltage range of 1.5 to 3 V. A) Evolution of the emission spectrum over time during the cycle vs. bias. B) Light intensity vs. applied bias. Arrows show the determination of the turn-on voltage. Scan rate = 0.01 V/s to ensure the response time of the LEC (up to 2 seconds) is negligible.

Electroluminescence (EL) (taken at a bias of 4 V) and photoluminescence (PL) spectra are shown in Figure 4.4. In both spectra the same features can be distinguished: a main peak, attributed to zero-phonon recombination, and a shoulder that is due to a two-phonon transition[43]. By fitting both curves with a double Gaussian (see section A.1), it was determined that the EL was blue shifted by 6 nm compared to the PL (maxima at 588 for EL and 594 for PL). This blueshift may be due to the absence of ions in the intrinsic part of the junction, where recombination takes place. An ion deficit may cause the polymers in the film to expand or contract, or could cause a difference in relative dielectric constant compared to an ion-rich region, changing the effective optical gap. Now that the device architecture has been optimized and it is known what results to expect from experiments on LECs, we will try to

produce devices based on QDs. In the upcoming sections, results from LECs based on ZnO and CdSe/CdS/ZnS QDs are presented and the viability of the two materials for use in LECs is analysed.

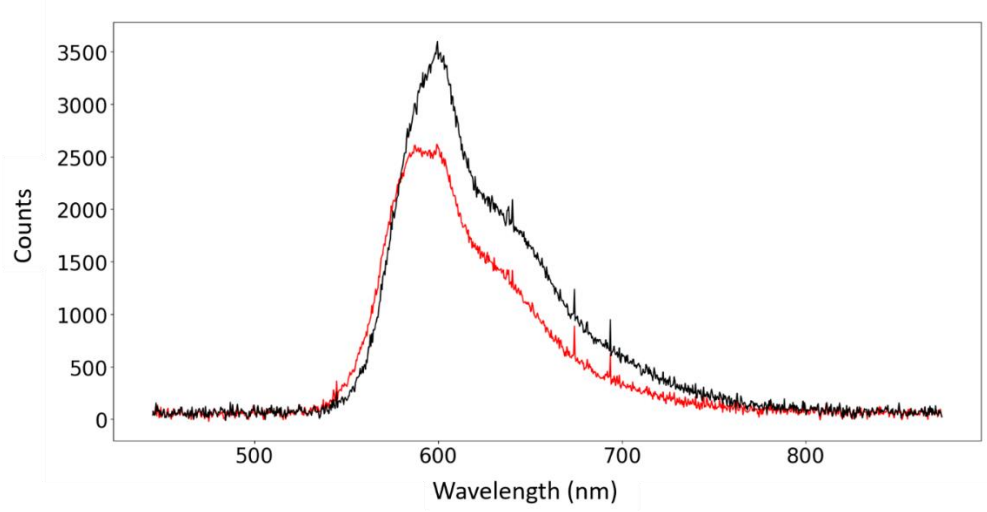

Figure 4.4. PL (black) and EL (red) spectrum of a MEH-PPV LEC. Maxima of the peaks are at 588 and 594 nm for EL and PL, respectively, indicating a blueshift of 6 nm for EL compared to PL.

4.3 LECs based on ZnO quantum dots

During testing the ZnO films showed significant conduction, but no light emission was observed. Because of this, a control device was produced without salt to obtain more information on the nature of the currents that were observed. The I-V curves of both the ZnO/PEO/$LiCF_3SO_3$ film and the control film are shown in Figure 4.5. The shape of the curve indicates that the device is rectifying, conducting more current when aluminium acts as the negative electrode rather than ITO. The current densities in the two films are similar, so the ions serve little or no role in the conduction mechanism. Since ZnO nanocrystals are intrinsic n-type conductors[44], they can conduct current without the necessity for doping, making them unsuitable candidates for LEC devices. For this reason, the focus from this point onward will be on CdSe QDs.

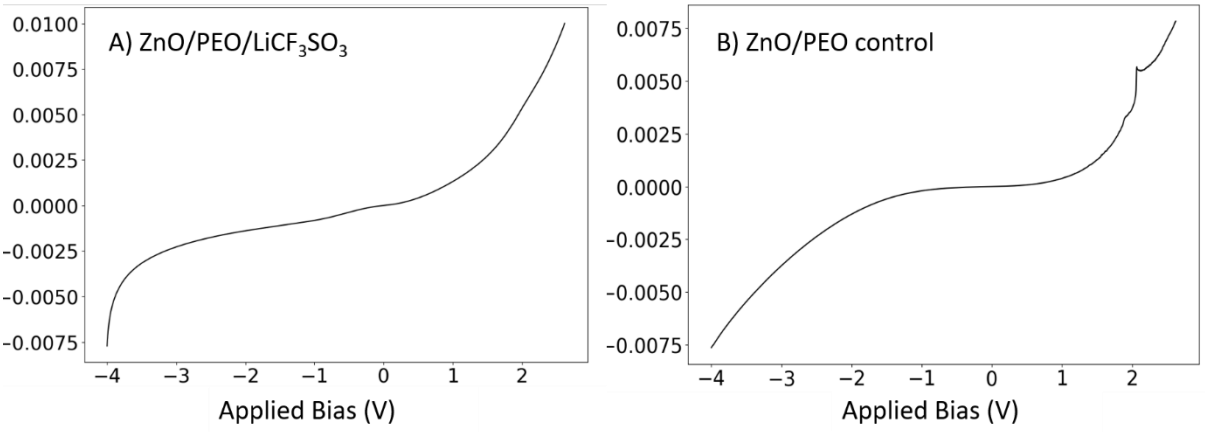

Figure 4.5. I-V curves of both a salt-rich ZnO/PEO film (A) and a control film without ions (B). ZnO nanoparticles conduct electrons even when no salt is present, making them unsuitable for use in LECs.

4.4 CdSe/CdS/ZnS ligand exchange

In order to reduce the interdot distance and improve the conductivity in the CdSe/CdS/ZnS QD films, a ligand exchange procedure was executed on the QDs. The goal was to exchange the native mixture of ligands that is present after synthesis (TOP, TOPO, OA, oleyamine and octanethiol) for the

short ligand pivalic acid. FTIR spectra of the CdSe/CdS/ZnS before and after the ligand exchange procedure are shown in Figure 4.6 (see section A.2 for the FTIR data of all ligands and solvents used in the preparation and ligand exchange of the quantum dots).

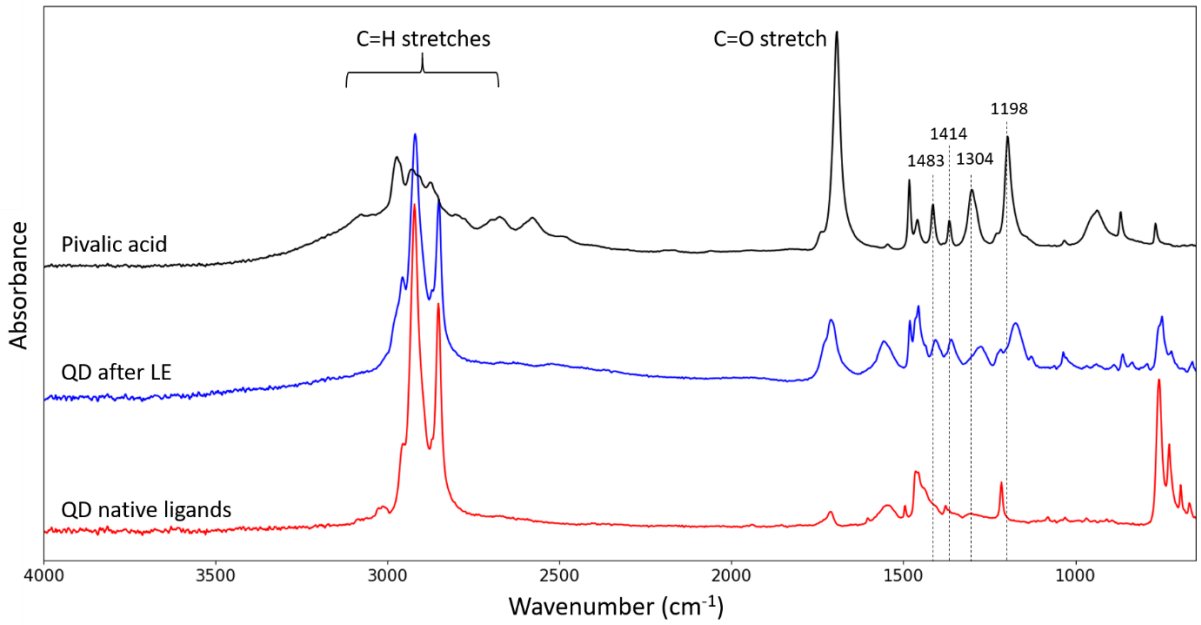

Figure 4.6. FTIR spectra of the native ligand QDs (red), QDs after ligand exchange procedure (blue) and pivalic acid (black). Although characteristic pivalic acid peaks can be observed in the spectrum after the ligand exchange procedure, the strong peaks in the C-H stretch region indicate that native ligands are still present and the ligand exchange procedure was at best partially successful.

The presence of strong C-H stretches in the spectrum indicates the presence of native ligands even after the ligand exchange procedure was completed. Characteristic pivalic acid peaks at 1483 cm^{-1} and 1414 cm^{-1} and slightly shifted peaks around 1304 cm^{-1} and 1198 cm^{-1} are however also present in the spectrum after ligand exchange, indicating the presence of pivalic acid. In addition, the carboxylic acid C=O stretch observed after ligand exchanged is reduced in intensity compared to the other peaks in the PA spectrum, which could mean (partial) deprotonation of the acid. It is plausible that some pivalic acid has been bound to the quantum dot surface, but the native ligands were certainly not fully removed. To confirm the presence of pivalic acid on the surface, NMR measurements could be taken. To completely strip the surface of native ligands and fully replace them with ligands of choice, a more thorough 2-phase ligand exchange procedure is suggested[27, 45]. This procedure will also allow for easy monitoring of the exchange.

4.5 LECs based on CdSe/CdS/ZnS quantum dots

An I-V scan of a device containing the CdSe/CdS/ZnS quantum dots which had undergone the ligand exchange procedure is plotted in Figure 4.7. Although the shape of the curve roughly reflects that of an LEC at least for $-6 < V < 0$, the current density is orders of magnitude lower than that observed in the MEH-PPV based LECs.

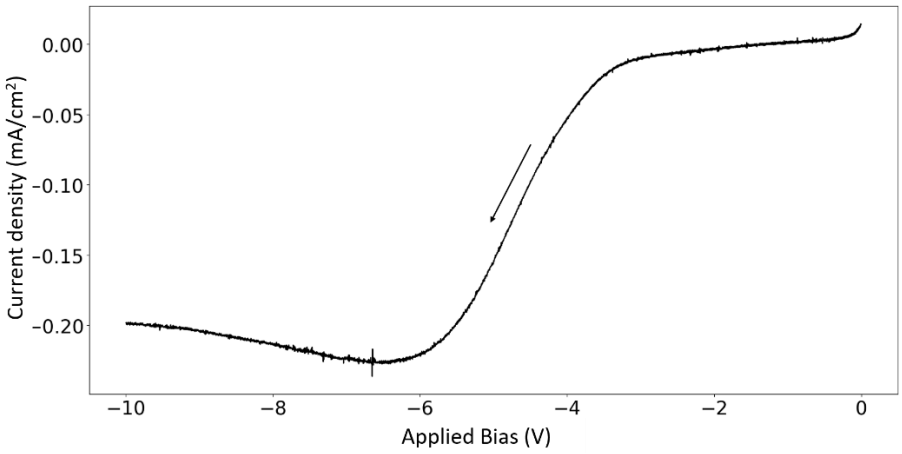

Figure 4.7. I-V curve of the CdSe/CdS/ZnS device. Scan rate = 0.01 V/s, scan direction indicated by the arrow. It is unclear whether the device operates as an LEC.

It is unclear whether the device functions as a real LEC or that the current is due to quantum dot conduction like in the ZnO film. CdSe/ZnS quantum dots films without the addition of an electrolyte have been shown to be able to conduct currents even magnitudes higher than the ones observed in our sample[38]. The current could thus entirely be due to electron conduction of the intrinsic quantum dots. Further research is needed to investigate the role of mobile ions in the conduction mechanism in quantum dot films. Although the ligand exchange procedure seems to enhance conduction somewhat, since the native ligand films were not able to conduct any current, improvements can be made in this regard. Increasing the packing density of the quantum dots, either through another ligand exchange procedure or crosslinking of the ligands, could enhance charge carrier mobility and thus increase conduction in quantum dot films. Further suggestions for improvement of the device can be found in section 5.3.

Computational results and discussion

In this chapter the results of drift-diffusion simulations of LEC devices are discussed. Section 5.1 gives insight in how to interpret the output of the simulations. The steady state concentration and potential profiles are presented as well as the transient current and recombination densities prior to reaching steady state. In section 5.2, the effects of different starting conditions on the simulations are analysed to show general trends that can be expected in LECs. A simulation that mirrors an experimental device is presented in section 5.3. Finally, in section 5.4 the I-V behaviour of simulated devices is discussed and compared with the experimental results from chapter 4.

5.1 Standard LEC

The steady state carrier concentrations, recombination profile and band structure in a simulated LEC with standard parameters at V_b = 2 V (see section 3.6) are plotted in Figure 5.1. The negative electrode is always positioned to the right of the device, while the positive electrode is on the left.

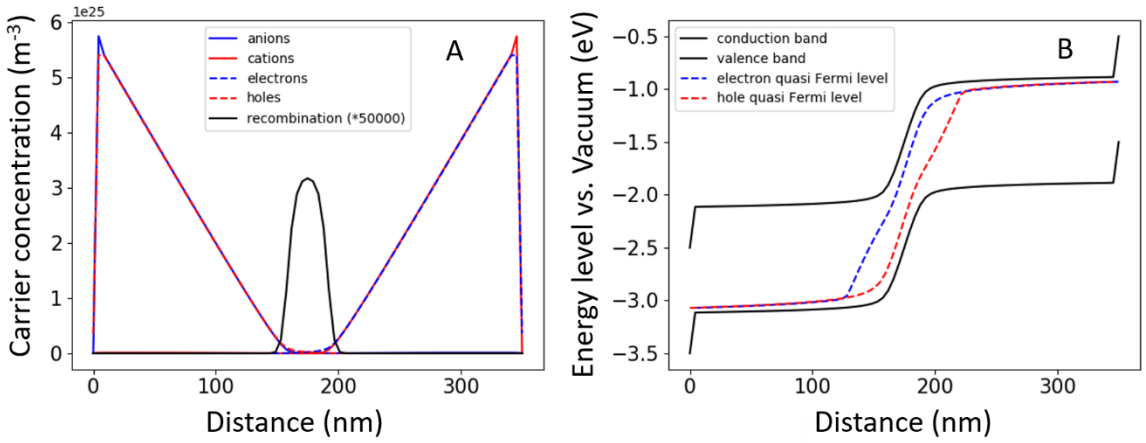

Figure 5.1. Computational results of a standard LEC. A) The carrier and recombination profile and B) the band structure of a simulated LEC device. p- and n-type doping can be observed on the left and right side of the device, respectively.

In the simulated devices at steady state, complete separation of ions has taken place as predicted by the ECD model: anions and cations have migrated to the left and right side of the device, respectively, where they electrically compensate the excess holes and electrons. This results in two opposite doping regimes and a p-i-n junction in the middle of the device, where all ions are depleted and recombination of the holes and electrons takes place. As can be seen in figure 5.1 A, the doping level is not constant throughout the device, but instead is at its maximum near the electrodes, then drops linearly over distance right up to the intrinsic region. In the doped regions, the electric field strength F is negligible, and thus the current is only due to diffusion. Since the current must be constant over the regions were no recombination takes place, it follows from equations 3.4 through 3.7 that the concentration of carriers must drop linearly over distance in the doped regions.

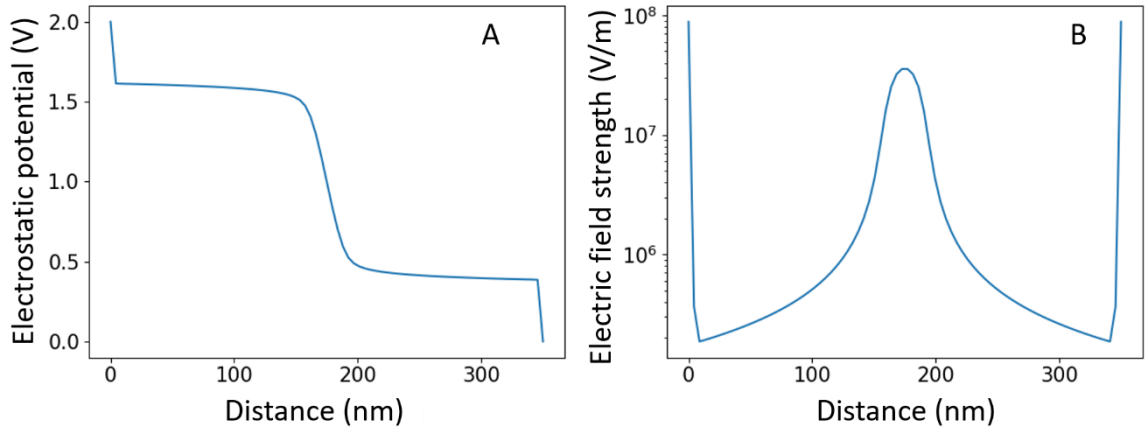

Figure 5.2. A) The potential profile and B) the electric field throughout a simulated device. Strong electric fields are present near the electrodes due to the EDLs and in the junction due to the unpaired holes and electrons.

The steady state potential and electric field profile are plotted in Figure 5.2, showing the presence of electric double layers (EDLs) near the electrodes, as well as a strong electric field at the position of the junction. The remainder of the potential that does not drop at the interface drops over the ion-free junction due to the unpaired holes and electrons. Due to the discrete nature of the simulation, the entire EDL is present in only one cell at the edge.

A simulation was run at 10 times resolution to give an indication of the actual ion concentration profile in the EDL (Figure 5.3 A). In this simulation, electron/hole injection was turned off and the applied potential was 1 V, so that the system would resemble two free electrodes in an electrolyte, with a potential drop of 0.5 V near both electrodes. Considering a cell width in the LEC simulations of ~4 nm, it is clear that the entire EDL and potential drop of 0.5 V would be present within the first cell.

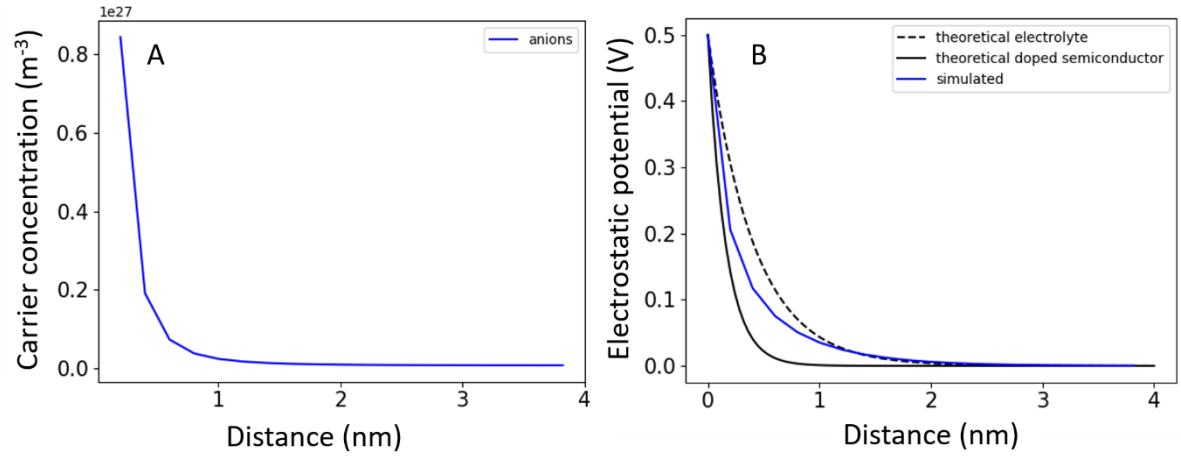

Figure 5.3. High resolution EDL simulations. A) Simulated ion concentration profile of an EDL. B) Simulated potential profile (blue) and theoretical prediction for the potential profile in an electrolyte (dotted black) and doped semiconductor (solid black) with the parameters used in the simulation. All models predict an EDL thickness of less than 4 nm.

Before doping has taken place, the system most closely resembles an electrolyte, while after the doping process is completed, it can be considered a doped semiconductor. The ion concentration before doping and the doping density near the interface that is obtained from the high-resolution simulation at steady state can be used to calculate the Debye length in the system according to equations A.1 and A.2 (section A.3). The Debye lengths can be used to predict the theoretical

exponential decay of the potential for the standard LEC before (Debye length = 0.41 nm for an ion concentration of $1.25*10^{25}$) and after doping (Debye length = 0.16 nm for a doping density of $5.4*10^{25}$) (Figure 5.3 B). Once the doping process is completed, the EDL becomes thinner because the doping level is at its maximum near the electrodes. Therefore, it can be expected that during the doping process in an LEC, the potential drop becomes more compact at the interface and as a result the electric field becomes stronger.

The number of ions in the EDL and thus the height of the potential drop at the electrodes is the result of an equilibrium between migration of ions and injection of charge carriers. At the start of the simulation, injection of holes and electrons is negligible because of the large injection barrier (i.e. the difference in energy between the level of the conduction/valence band and the Fermi level inside the negative/positive electrode). When the simulation starts ions move towards the opposite electrode, and accumulate at the interface to form an EDL since they cannot leave the device. Due to the unpaired ions in the EDL next to the electrodes some of the charge in the electrodes is 'shielded' from the perspective of the charges inside the device. This results in a strong electric field and a drop in electrostatic potential at the interface of the materials, which in turn causes strong band bending, bringing the energy level of conduction and valence bands closer to the Fermi level in the electrode and therefore decreasing the injection barrier (Figure 5.1 B).

The more ions accumulate, the more of the charge in the electrode is 'shielded', creating a difference in electrostatic potential for electrons, which lowers the effective injection barrier that the charge carriers experience. The EDL continues to develop until the injection barrier is lowered enough that the injection of holes/electrons is equal to the flux of ions towards the electrode (Figure 5.4). After this point, the ions start matching up with the excess charge carriers and the doping process ensues and continues until all the ions are either in an EDL or matched with a hole/electron. Doping leads to a temporary increase in current density as many electrons and holes enter the system to match up with the ions. Once the doping process is completed, the current density decreases until only the recombination current remains, and the device reaches steady state where the current density *J* is equal to the recombination density times the elementary charge (*q*R)*.

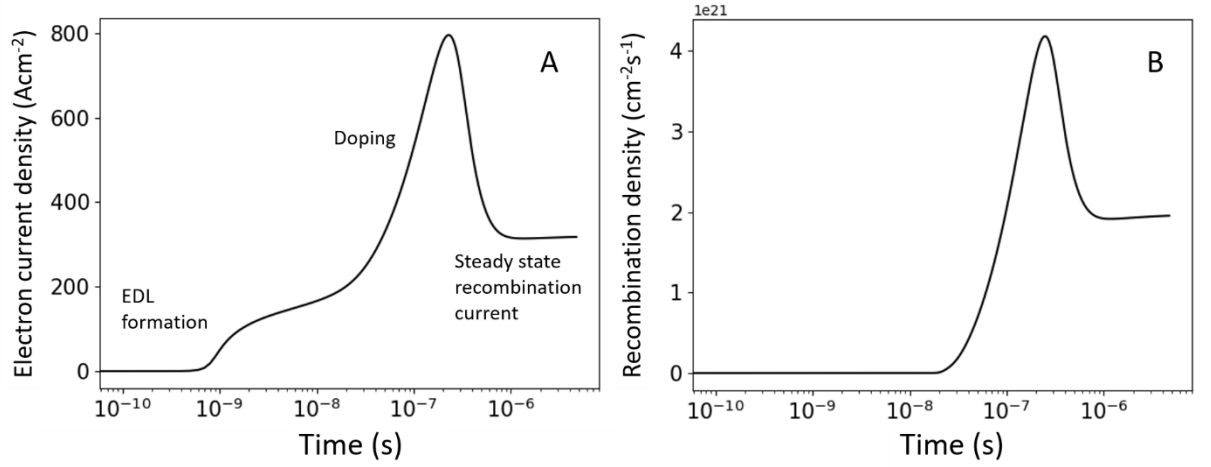

Figure 5.4. Transient current and recombination density in an LEC. A) The electron current in a simulated device over time. B) The total recombination in the device over time. The current density starts increasing after the EDLs have fully developed. After EDL formation a temporary increase in current density can be observed as the doping process takes place. When doping is complete the system reaches steady state. Note that while the units provided correspond to actual predictions by the model, the starting parameters do not resemble a physical system, so only qualitative trends can be examined.

5.2 General trends in LECs

In order to get more insight in the operation mechanisms of LECs and develop ideas to improve the experimental devices, predictions were made for general trends in LECs by changing a single parameter in the simulation while keeping all others the same. The effects of asymmetrical injection barriers, unequal hole and electron mobilities and different salt concentrations were examined because they were deemed to be the most relevant for the optimization of experimental devices. All the effects discussed in this section will also appear in the simulated quantum dot LEC in section 5.3.

5.2.1 Asymmetrical injection barriers

Since the initial injection barrier is equal to the difference between the work function of the positive/negative electrode material and the energy level of the valence/conduction band edge, changing the initial injection barriers gives insight in how the devices would operate when different electrode materials are used. In experimental devices, it is expected that the injection barriers for holes will be different than the one for electrons, so to mirror this asymmetrical injection barriers were used in the simulation. By increasing the Fermi level in both electrodes and the semiconductor itself by 0.2 eV, the initial injection barriers were rendered asymmetrical (0.3 eV for electrons, 0.7 eV for holes, instead of equal 0.5 eV barriers for both). The steady state carrier concentration, the potential profiles, hole/electron currents and recombination density vs. time from this simulation are plotted in Figure 5.5.

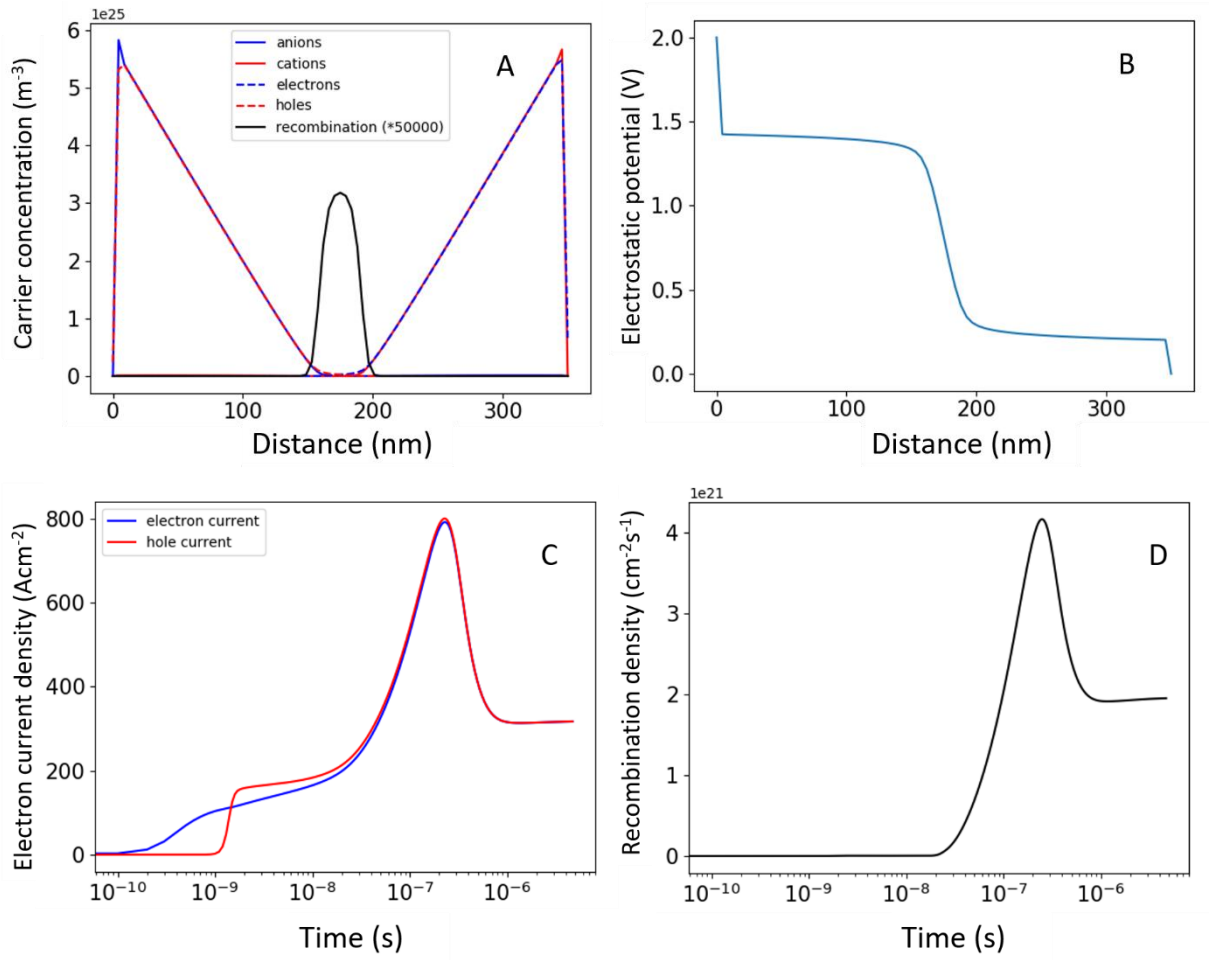

Figure 5.5. The characteristics of a simulated LEC with a higher injection barriers for holes than electrons. A) Steady state concentration profile. B) Potential profile. The difference in injection barriers can be identified in this plot by the potential drops at the sides of the device. C) Electron and hole current densities in the device vs. time. Electron injection starts well before any hole injection has taken place. D) Recombination density vs. time. The steady state recombination density is independent of the height of the initial injection barriers in LECs.

The only change in the steady state profile that arises from the difference in injection barriers is the number of ions in the EDL. The higher the barrier, the more ions need to accumulate before the barrier is lowered enough to allow injection of carriers. The fact that more ions are present in the EDL also means less of them will be available for doping in the device, but this difference is typically negligible at the ion concentrations used in these simulations. An important advantage of LECs over classical LEDs that becomes apparent from these graphs is that the steady state current density and recombination density do not depend on the initial injection barriers. In LEDs, electrode materials must be carefully chosen to minimize the injection barriers, while in LECs, as long as the applied bias is sufficiently high, the injection barriers can be negated entirely by the formation of the EDLs. It should be noted that if the contacts are perfect (i.e. the injection barrier is exactly equal to the energy difference between the work function of the metal and the band energy in the semiconductor), the turn-on voltage does not depend on the injection barriers either but is always equal to the bandgap of the semiconductor. Since the open circuit voltage is equal to the difference in work functions of the electrode materials, even if both injection barriers are very high, the difference between the open circuit voltage and the applied bias compensates for this.

5.2.2 Unequal electron and hole mobility

So far devices with equal hole and electron mobility have been considered, but this scenario is highly unlikely in experimental semiconductor materials. In bulk CdSe for example the difference between hole and electron mobilities is almost an order of magnitude[46]. To find out which effect the difference in mobility has on the functioning of the LECs, a device with $\mu_n = 10*\mu_p$ was simulated, the characteristics of which are shown in Figure 5.6.

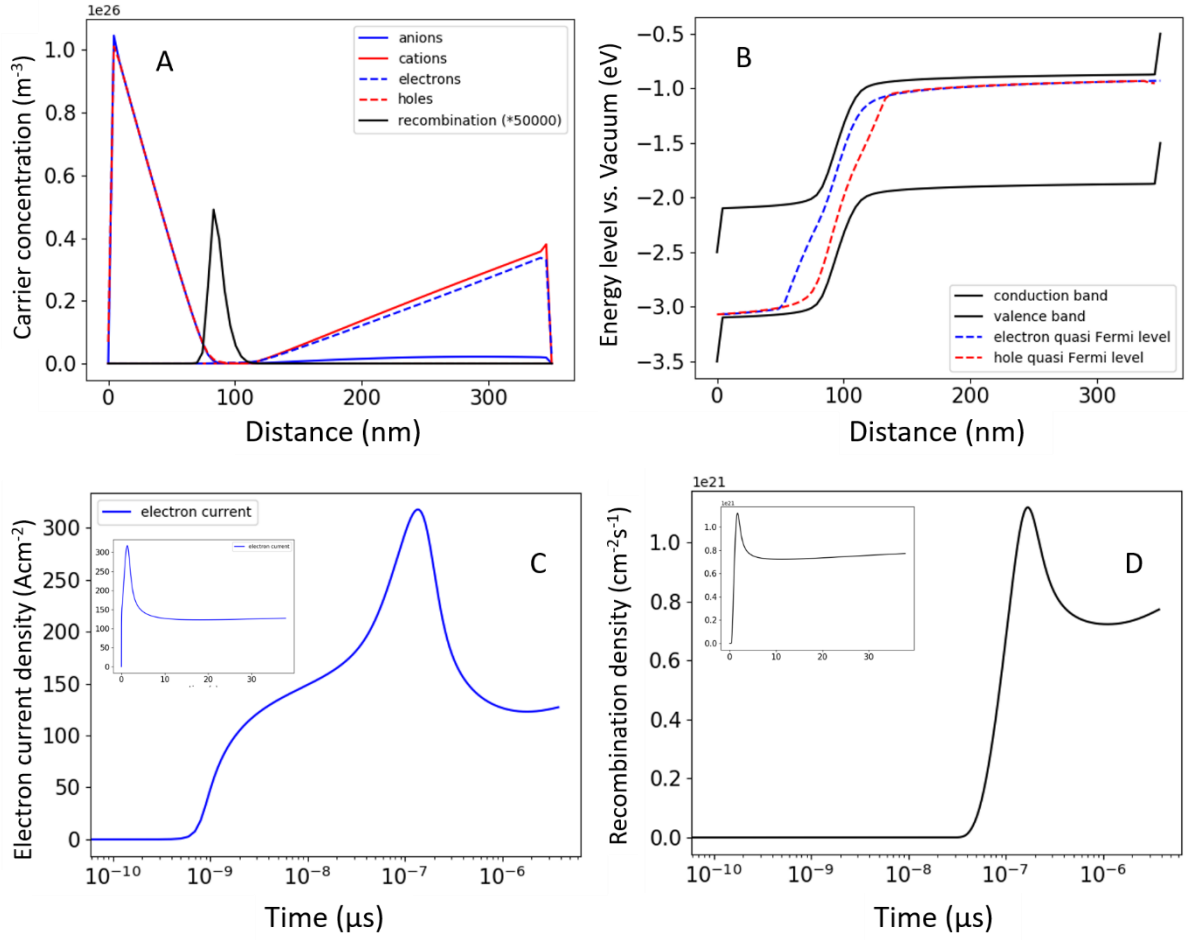

Figure 5.6. The characteristics of a simulated device where $\mu_n = 10*\mu_p$. The position of the junction is a function of the mobility difference. Electron current and recombination density vs. linear time are included in the inset to more convincingly show that steady state has almost been reached.

As can be observed in Figure 5.6 A and B, the charge carrier recombination zone moves towards the electrode with lower charge carrier mobility. Since the hole current in the p-doped region and the electron current in the n-doped region are equal, the difference in carrier mobilities must be compensated for by a difference in doping density, resulting in the asymmetrical doping profile in figure 5.6 A. The steady state current and recombination densities are lower in comparison to the case with equal mobility firstly because the recombination intensity scales linearly with the sum of the mobilities (equation 3.8) and secondly because the cations are spread out over a larger distance, so the doping level for electrons is lower, limiting the electron current density. As expected, lower carriers mobilities thus lead to lower steady state current and less light emission. Because the lower hole mobility greatly increases the time it takes to reach steady state for the device, the simulation was not run all the way to steady state but interrupted once the trends were clear.

5.2.3. Ion concentration

In experimental devices, the ion concentration can easily be adjusted by changing the amount of salt that is added to the active layer, so finding an optimal concentration could be an easy way to improve performance. The characteristics of a simulated LEC with an ion concentration of $1.25*10^{24}$ m^{-3} (10 times lower than the standard) are plotted in Figure 5.7. The most important effect of the lower concentration is the decreased doping level in the device. This lower doping density also leads to a lower steady state recombination rate and a wider recombination zone. Although the results from the simulation may suggest the most optimal device is one with an ion concentration as high as possible, in practice unwanted electrochemical side reactions at the negative electrode and doping-induced exciton quenching will hamper the light emission efficiency at high ion concentrations[47, 48]. In experiments, increasing the ion concentration also goes along with an increase of the mass fraction of the electrolyte in the active layer of the device, which may additionally reduce the mobility of holes and electrons in the semiconductor.

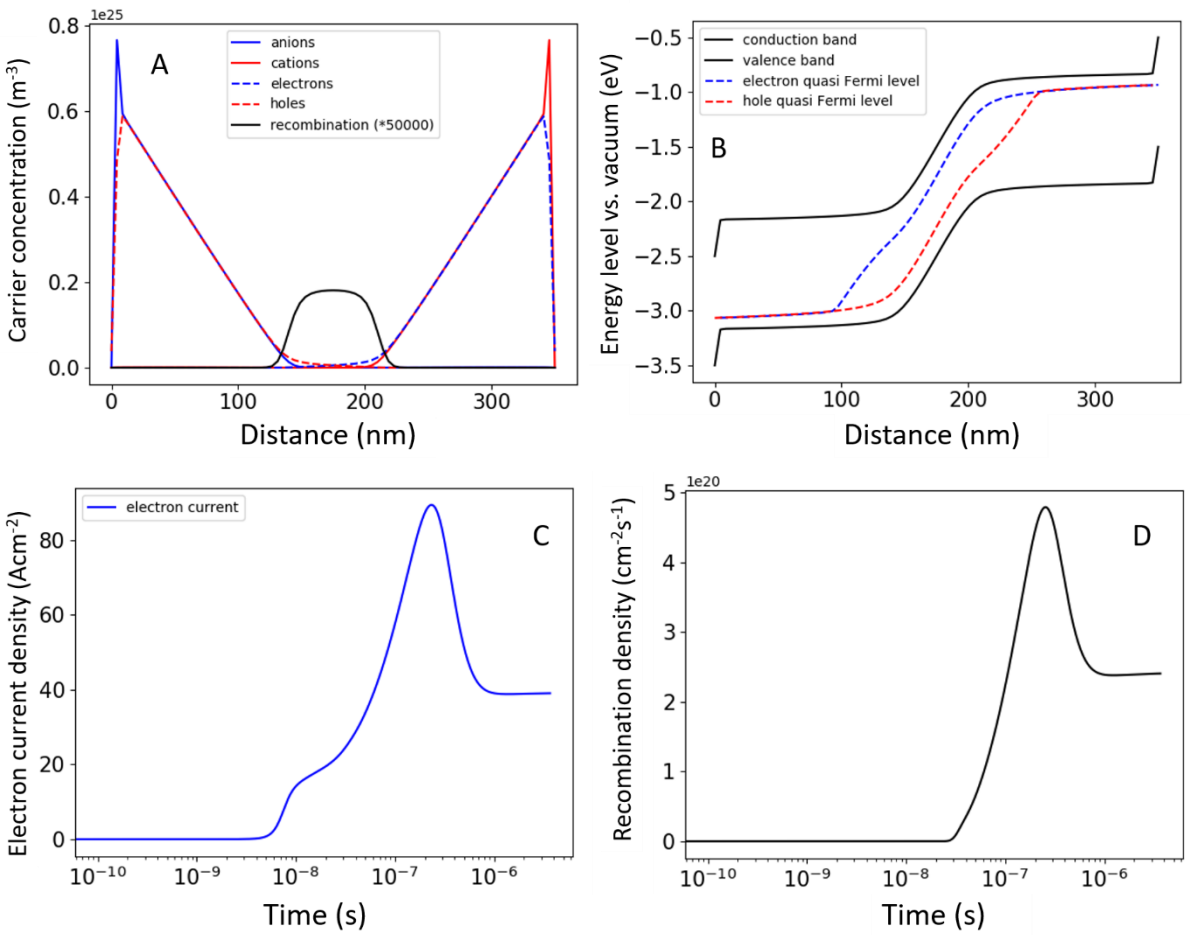

Figure 5.7. The characteristics of a simulated device with a lower ion concentration. The doping density in these devices is limited, leading to lower current and recombination densities.

5.3 LEC with CdSe parameters

Now that the output of the simulations is familiar and the effects of adjusting some starting parameters have been discussed, we can run a simulation that mirrors the experimental devices. The results of three different types of simulations resembling CdSe LECs are shown in Figure 5.9. All simulations were run at an applied bias V_b = 4 V. Because the work function of aluminium lies above the conduction band edge there is no injection barrier for electrons in the devices with an aluminium electrode, resulting in an immediate influx of electrons and a high initial electron current (Figure 5.9 A

& B). The current then decreases as the EDLs develop and the electric field in the device is reduced. Once the EDL at the positive electrode is fully developed, hole injection starts, doping occurs and the device reaches steady state similarly to the devices with standard parameters. In the device with unequal mobilities (Figure 5.9 B), the doping process is spread out over a longer time so that the increase in current density that is normally observed during doping is much less pronounced.

In the device with a gold electrode, the EDL at the negative electrode must first be developed before electron injection can take place, after which the device shows the same behaviour as that with the aluminium electrode. The steady state current in all devices is lower than that of the standard parameter device, as can be expected from the lower mobilities of charge carriers. However, the currents predicted by the model are 7-8 orders of magnitude higher than those observed is the experimental devices (section 4.5). Possible explanations for this could be that the charge carrier mobility in real films is even lower than the values used in the simulation, that traps in the quantum dots limit the current density, or that only part of the ions is mobile enough to migrate and contribute to the doping due to an inhomogeneous microstructure if the quantum dots coagulate. Additionally, when an aluminium electrode is used, the difference in initial injection barriers is 1.8 eV. In the theoretical simulations, this difference does not impede with the development of a p-i-n junction, as hole injection is eventually facilitated by the formation of a large EDL. However, in reality the large difference in injection barrier may have a negative effect on operation. The difference in barriers could be minimized by shifting the band edges towards a higher level by means of ligand exchange. Additionally, for the development of quantum dot LECs, it is recommended to use short ligands and a high packing density of the quantum dots in the film, to achieve the maximum charge carrier mobility.

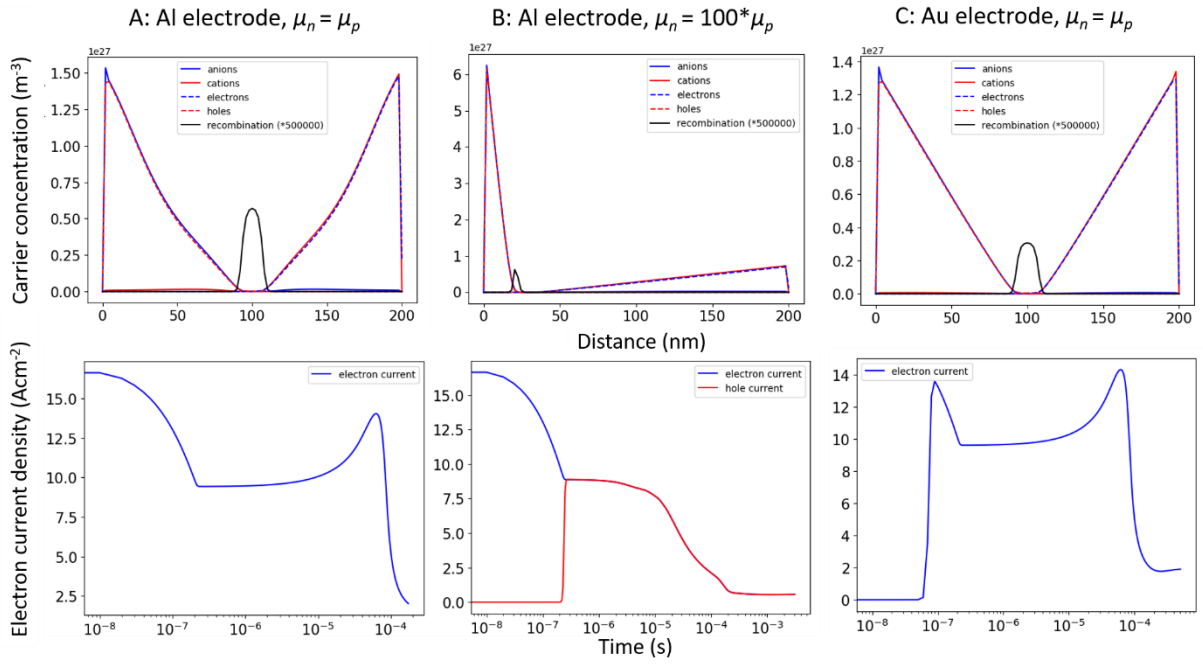

Figure 5.9. Characteristics of simulated devices with CdSe parameters. A) Aluminium electrode, equal hole and electron mobilities. Because the injection barrier for electrons is low, the initial electron current is high. B) Aluminium electrode, $\mu_n = 100*\mu_p$. Due to the large difference in mobilities, the doping process takes a longer time and the current peak before reaching steady state is flattened out. C) Gold electrode, equal hole and electron mobilities. Electron injection only starts once the EDL at the negative electrode is fully developed.

5.4 I-V trends in LECs

To finish the comparison of the simulations with the experimental devices, the I-V curves of devices with CdSe and standard parameters were simulated by increasing the applied bias with a small increment (0.1 V) once the system had reached steady state. These I-V curve are plotted in Figure 5.10.

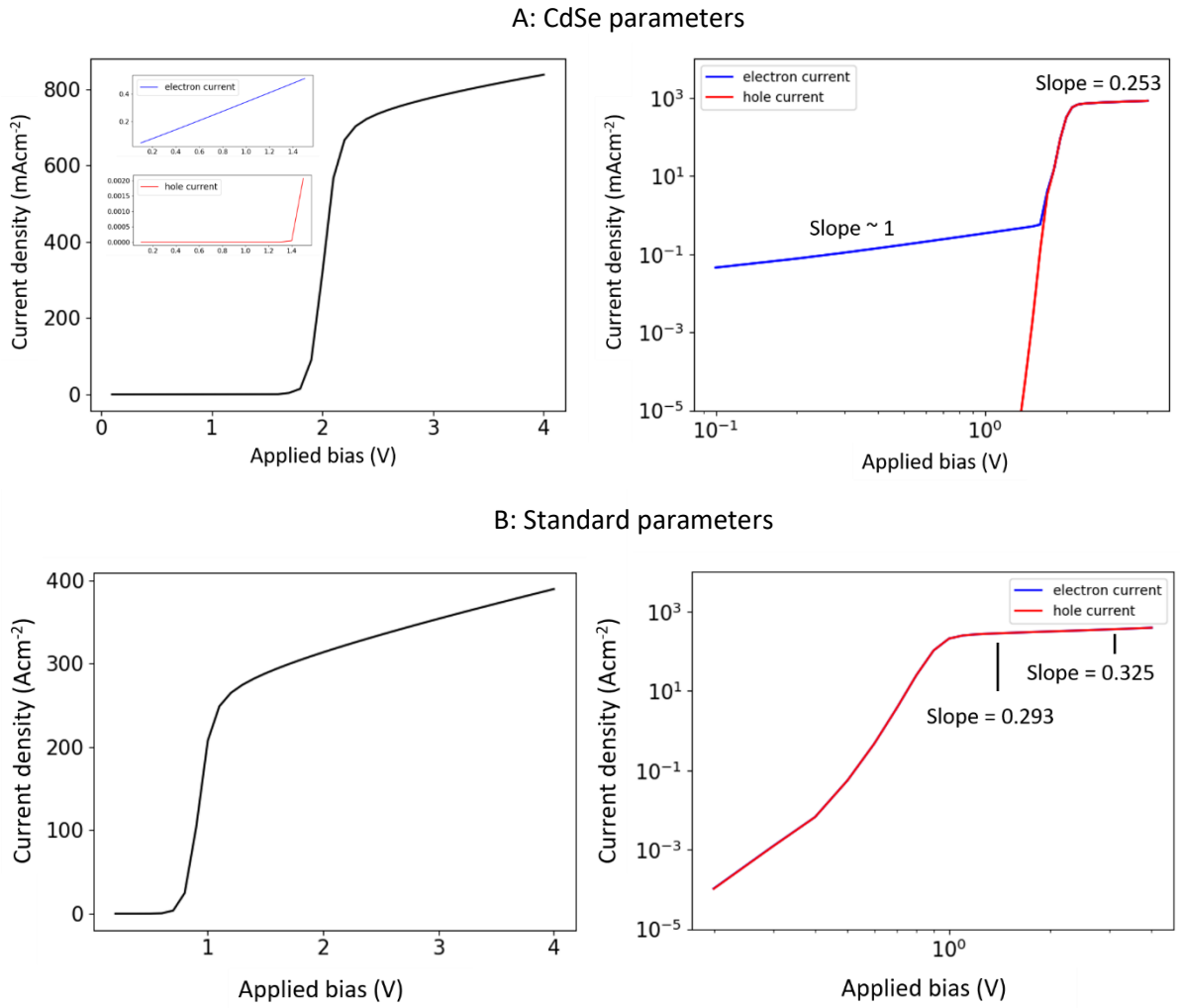

Figure 5.10. I-V characteristics of a simulated CdSe (A) and standard (B) LEC. The current behaviour of holes and electrons separately for bias lower than 1.5 V in the CdSe LEC is shown in the insets. Pre- and post-doping regimes are distinguished by different voltage dependence of the current.

In the CdSe LEC at applied voltages significantly lower than the bandgap of the semiconductor (V_b < 1.7 V), the I-V behaviour for holes is exponential. The height of the EDL and thus the reduction of the injection barrier scales linearly with the applied bias, which results in an exponential increase of hole concentration in the device as governed by the modified Boltzmann injection model (equation 3.2). Hole injection is thus limiting in the device for low applied bias. The electron current in the same voltage regime increases linearly with applied bias (slope = 0.97 in the double log plot). Because of the low electron injection barrier, electrons can flow into the device freely. There is no electric field present at low bias (all the potential drops at the interface), so the electron current is diffusion-limited. As more anions migrate to take part in the EDL at the positive electrode, more electrons can take their place, leading to some minor n-type doping and an increase in the diffusion current. Since the EDL grows linearly with applied bias, a linear increase in the electron current is expected. At applied bias close to the bandgap of the material, the current density increases rapidly with voltage as doping occurs and the junction is formed.

When the applied bias is significantly larger than the bandgap, the electron and hole current are equal. The current density in the CdSe device had an average voltage dependence of $J \sim V^{0.253}$ in this regime as determined by the slope in the double log plot. This voltage dependence can be explained by expansion of the junction (Figure 5.11). Once the EDLs are fully developed, any increase in the applied bias results in an equal increase in the potential drop in the recombination zone and an increase in the drift-current density there according to equations 3.4 and 3.5 (Figure 5.11 B) If the recombination zone width would remain the same, the electric field strength and current density in the junction would increase linearly with the applied bias. However, since the current density must be constant over the device, the diffusion currents in the doped regions must also increase. This increase is facilitated by a rearrangement of the ions closer to the electrodes, so that the junction becomes wider and the gradient in the doping density is steeper (Figure 5.11 C). Due to this widening, the electric field strength and the current density in the recombination zone scale with the applied bias according to $J \sim V^{\alpha}$, where $0 < \alpha < 1$. α is not a constant but depends itself on the applied bias and the type of LEC that is considered (Table 5.1). The I-V behaviour at applied bias higher than the band gap is thus complex and should be determined experimentally for a certain device. This would also imply that fixing the ions in a LEC device (section 2.3), would introduce a certain maximum current density, as the recombination zone width would be fixed as well.

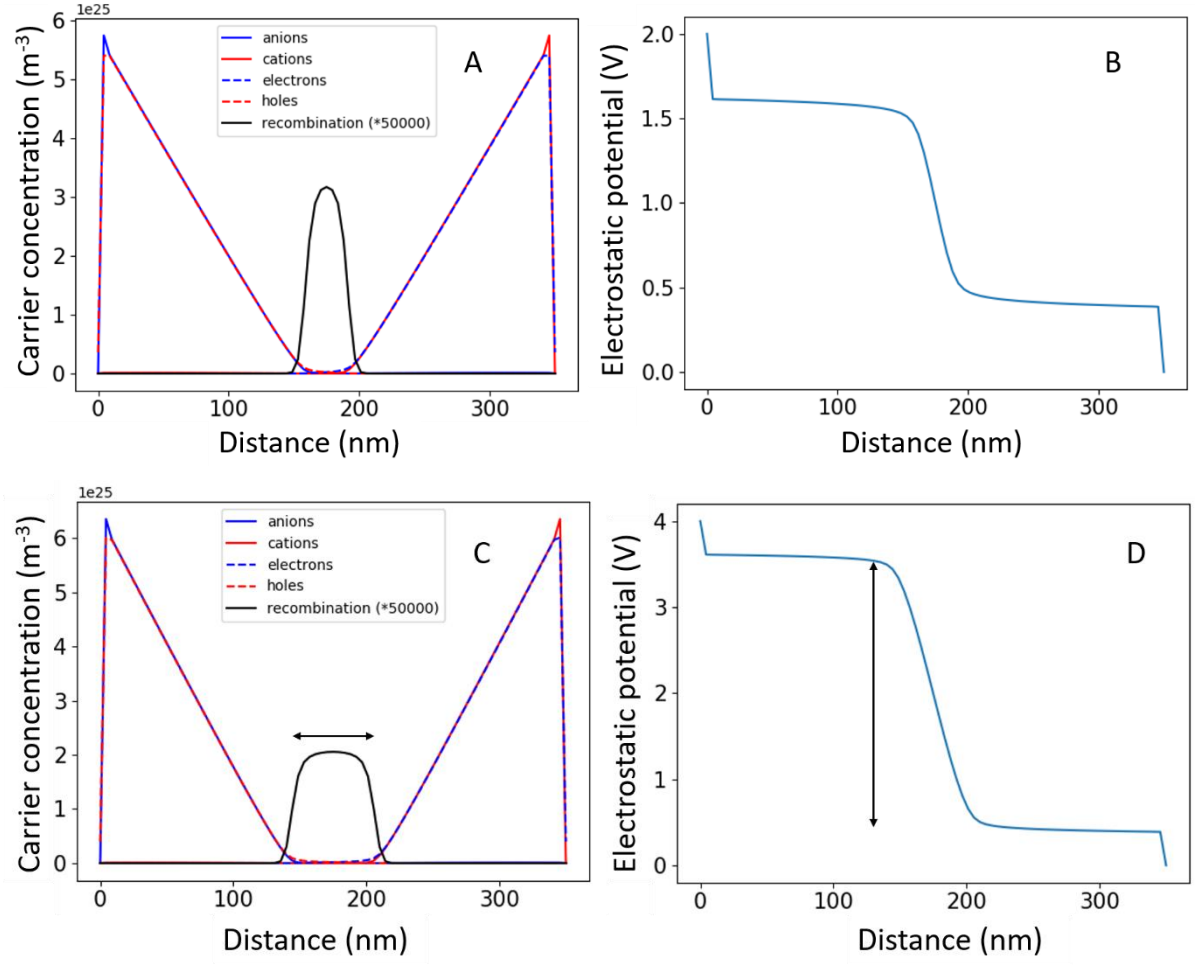

Figure 5.11. Comparison of steady state characteristics for different applied bias in the standard LEC. A) Carrier concentration and B) potential profile for V_b = 2V. C) Carrier concentration and D) potential profile for V_b = 4V. For a higher applied bias a larger potential drop in the recombination zone and a larger width of the recombination zone are observed.

Table 5.1. Double log-slopes in simulated CdSe and standard parameters devices. No patterns were found in the slope data.

$(V_b - E_g)$	0.5	1	1.5	2	2.5	3
I-V double log slope standard LEC	0.322	0.286	0.296	0.313	0.332	0.352
I-V double log slope CdSe LEC	0.581	0.303	0.272	-	-	-

Although it is inverted compared to the experimental data, since the model cannot apply a negative bias, the simulated CdSe I-V curve shows remarkable similarity to the experimental curve of the CdSe/CdS/ZnS LEC (section 4.5). In the experimental curve for V_b < 3.5 V, the linear behaviour could correspond to the formation of the EDLs, and the sharp increase in current density for 3.5 V < V_b < 6 V to the doping of the device. A drop-off of the current density at higher applied bias is also present in both curves. However, more experiments need to be done to confirm that doping has actually taken place in the quantum dot LEC films.

Conclusion and future outlook

Trends in LECs were examined by analysing experimental and simulated devices. LECs based on MEH-PPV were successfully produced and showed typical I-V and luminescence behaviour. ZnO nanoparticles were found to be unsuitable for use in LECs due to their high inherent n-type doping level. CdSe/CdS/ZnS QD/PEO/$LiCF_3SO_3$ films were found to conduct very little current and did not emit any light. From computational simulations, it was found that as long as the difference between hole and electron injection barriers is not too large, the choice of electrode material likely has little influence on the operation of LECs. Hole and electron mobility were identified as important parameters for making an efficient, bright LEC. Improving the poor conduction in CdSe quantum dots by reducing the interdot distance should be the first step on the road to producing quantum dot LECs. While it is likely impossible in normal films, a unique opportunity to observe hole conduction in quantum dots is presented in LEC devices, since the presence of an EDL can negate the large hole injection barrier. To facilitate hole injection, ligand exchange may be used to shift the valence band as high as possible relative to vacuum, so that the hole injection barrier is minimal. Kelvin probe microscopy techniques could be used to visualise the potential profile and aid in analysing the doping process in the devices.

References

1. Pei, Q., et al., *Polymer light-emitting electrochemical cells.* Science, 1995. **269**(5227): p. 1086-1088.
2. Lee, J.K., et al., *Thin film light emitting devices from an electroluminescent ruthenium complex.* Applied physics letters, 1996. **69**(12): p. 1686-1688.
3. Mekis, I., et al., *One-pot synthesis of highly luminescent CdSe/CdS core− shell nanocrystals via organometallic and "Greener" chemical approaches.* The Journal of Physical Chemistry B, 2003. **107**(30): p. 7454-7462.
4. Park, Y.-S., et al., *Near-unity quantum yields of biexciton emission from CdSe/CdS nanocrystals measured using single-particle spectroscopy.* Physical review letters, 2011. **106**(18): p. 187401.
5. de Mello Donega, C., et al., *Single-step synthesis to control the photoluminescence quantum yield and size dispersion of CdSe nanocrystals.* The Journal of Physical Chemistry B, 2003. **107**(2): p. 489-496.
6. Caruge, J., et al., *Colloidal quantum-dot light-emitting diodes with metal-oxide charge transport layers.* Nature photonics, 2008. **2**(4): p. 247.
7. Mocatta, D., et al., *Heavily doped semiconductor nanocrystal quantum dots.* Science, 2011. **332**(6025): p. 77-81.
8. Schimpf, A.M., et al., *Electronic doping and redox-potential tuning in colloidal semiconductor nanocrystals.* Accounts of chemical research, 2015. **48**(7): p. 1929-1937.
9. Guyot-Sionnest, P., *Charging colloidal quantum dots by electrochemistry.* Microchimica Acta, 2008. **160**(3): p. 309-314.
10. Neamen, D.A., *Semiconductor Physics and Devices*. 2012: McGraw-Hill Education.
11. By TheNoise at English Wikipedia, C.B.-S., https://commons.wikimedia.org/w/index.php?curid, 2020.
12. Reiss, P., M. Protiere, and L. Li, *Core/shell semiconductor nanocrystals.* small, 2009. **5**(2): p. 154-168.
13. Shim, M. and P. Guyot-Sionnest, *N-type colloidal semiconductor nanocrystals.* Nature, 2000. **407**(6807): p. 981.
14. Koh, W.-k., et al., *Heavily doped n-type PbSe and PbS nanocrystals using ground-state charge transfer from cobaltocene.* Scientific reports, 2013. **3**: p. 2004.
15. Rinehart, J.D., et al., *Photochemical electronic doping of colloidal CdSe nanocrystals.* Journal of the American Chemical Society, 2013. **135**(50): p. 18782-18785.
16. Schimpf, A.M., et al., *Controlling carrier densities in photochemically reduced colloidal ZnO nanocrystals: size dependence and role of the hole quencher.* Journal of the American Chemical Society, 2013. **135**(44): p. 16569-16577.
17. Guyot-Sionnest, P., *Colloidal quantum dots.* Comptes Rendus Physique, 2008. **9**(8): p. 777-787.
18. Yu, D., C. Wang, and P. Guyot-Sionnest, *n-Type conducting CdSe nanocrystal solids.* Science, 2003. **300**(5623): p. 1277-1280.
19. Kagan, C.R. and C.B. Murray, *Charge transport in strongly coupled quantum dot solids.* Nature nanotechnology, 2015. **10**(12): p. 1013-1026.
20. Gao, Y., et al., *Photoconductivity of PbSe quantum-dot solids: dependence on ligand anchor group and length.* ACS nano, 2012. **6**(11): p. 9606-9614.
21. Guyot-Sionnest, P. and C. Wang, *Fast voltammetric and electrochromic response of semiconductor nanocrystal thin films.* The Journal of Physical Chemistry B, 2003. **107**(30): p. 7355-7359.
22. Wang, Z., et al., *Enhancement of charge transport in quantum dots solar cells by N-butylamine-assisted sulfur-crosslinking of PbS quantum dots.* Solar Energy, 2018. **174**: p. 399-408.

23. Steiner, D., et al., *Level structure of InAs quantum dots in two-dimensional assemblies.* Nano letters, 2006. **6**(10): p. 2201-2205.
24. Artemyev, M., et al., *Evolution from individual to collective electron states in a dense quantum dot ensemble.* Physical Review B, 1999. **60**(3): p. 1504.
25. Maness, K.M., et al., *Solid-state diode-like chemiluminescence based on serial, immobilized concentration gradients in mixed-valent poly [Ru (vbpy) 3](PF6) 2 films.* Journal of the American Chemical Society, 1996. **118**(43): p. 10609-10616.
26. Norell Bader, A.J., et al., *Precise color tuning via hybrid light-emitting electrochemical cells.* Nano letters, 2010. **11**(2): p. 461-465.
27. Qian, G., et al., *Saturated and Multi-Colored Electroluminescence from Quantum Dots Based Light Emitting Electrochemical Cells.* Advanced Functional Materials, 2014. **24**(28): p. 4484-4490.
28. DeMello, J., et al., *Ionic space-charge effects in polymer light-emitting diodes.* Physical Review B, 1998. **57**(20): p. 12951.
29. Matyba, P., et al., *The dynamic organic p–n junction.* Nature materials, 2009. **8**(8): p. 672-676.
30. van Reenen, S., et al., *A unifying model for the operation of light-emitting electrochemical cells.* Journal of the American Chemical Society, 2010. **132**(39): p. 13776-13781.
31. Leger, J.M., D.B. Rodovsky, and G.P. Bartholomew, *Self-Assembled, Chemically Fixed Homojunctions in Semiconducting Polymers.* Advanced Materials, 2006. **18**(23): p. 3130-3134.
32. Gao, J., G. Yu, and A.J. Heeger, *Polymer light-emitting electrochemical cells with frozen pin junction.* Applied physics letters, 1997. **71**(10): p. 1293-1295.
33. Yu, G., et al., *Polymer Light-Emitting Electrochemical Cells with Frozen p-i-n Junction at Room Temperature.* Advanced Materials, 1998. **10**(5): p. 385-388.
34. Gudjonsdottir, S., et al., *The role of dopant ions on charge injection and transport in electrochemically doped quantum dot films.* Journal of the American Chemical Society, 2018. **140**(21): p. 6582-6590.
35. Qu, L., Z.A. Peng, and X. Peng, *Alternative routes toward high quality CdSe nanocrystals.* Nano letters, 2001. **1**(6): p. 333-337.
36. Greaney, M.J., et al., *Effects of interfacial ligand type on hybrid P3HT: CdSe quantum dot solar cell device parameters.* The Journal of chemical physics, 2019. **151**(7): p. 074704.
37. Li, X., J. Gao, and G. Liu, *Thickness dependent device characteristics of sandwich polymer light-emitting electrochemical cell.* Organic Electronics, 2013. **14**(6): p. 1441-1446.
38. Hikmet, R., D. Talapin, and H. Weller, *Study of conduction mechanism and electroluminescence in CdSe/ZnS quantum dot composites.* Journal of Applied Physics, 2003. **93**(6): p. 3509-3514.
39. Modestov, M., et al., *Model of the electrochemical conversion of an undoped organic semiconductor film to a doped conductor film.* Physical Review B, 2010. **81**(8): p. 081203.
40. Klein, R.J., et al., *Modeling electrode polarization in dielectric spectroscopy: Ion mobility and mobile ion concentration of single-ion polymer electrolytes.* The Journal of chemical physics, 2006. **124**(14): p. 144903.
41. Pei, Q., et al., *Polymer light-emitting electrochemical cells: in situ formation of a light-emitting p– n junction.* Journal of the American Chemical Society, 1996. **118**(16): p. 3922-3929.
42. Yu, G., et al., *Measurement of the energy gap in semiconducting polymers using the light-emitting electrochemical cell.* Chemical physics letters, 1996. **259**(3-4): p. 465-468.
43. Marletta, A., V. Goncalves, and D.T. Balogh, *Photoluminescence of MEH-PPV/PS blends.* Brazilian Journal of physics, 2004. **34**(2B): p. 697-698.
44. Jagadish, C. and S.J. Pearton, *Zinc oxide bulk, thin films and nanostructures: processing, properties, and applications*. 2011: Elsevier.

45. Dong, A., et al., *A generalized ligand-exchange strategy enabling sequential surface functionalization of colloidal nanocrystals.* Journal of the American Chemical Society, 2010. **133**(4): p. 998-1006.
46. Canali, C., et al., *Hole and electron drift velocity in CdSe at room temperature.* Solid State Communications, 1972. **11**(1): p. 105-107.
47. Fang, J., et al., *Identifying and alleviating electrochemical side-reactions in light-emitting electrochemical cells.* Journal of the American Chemical Society, 2008. **130**(13): p. 4562-4568.
48. Fang, J., P. Matyba, and L. Edman, *The design and realization of flexible, long-lived light-emitting electrochemical cells.* Advanced Functional Materials, 2009. **19**(16): p. 2671-2676.

Appendix

A.1 Fit of the MEH-PPV EL and PL spectra

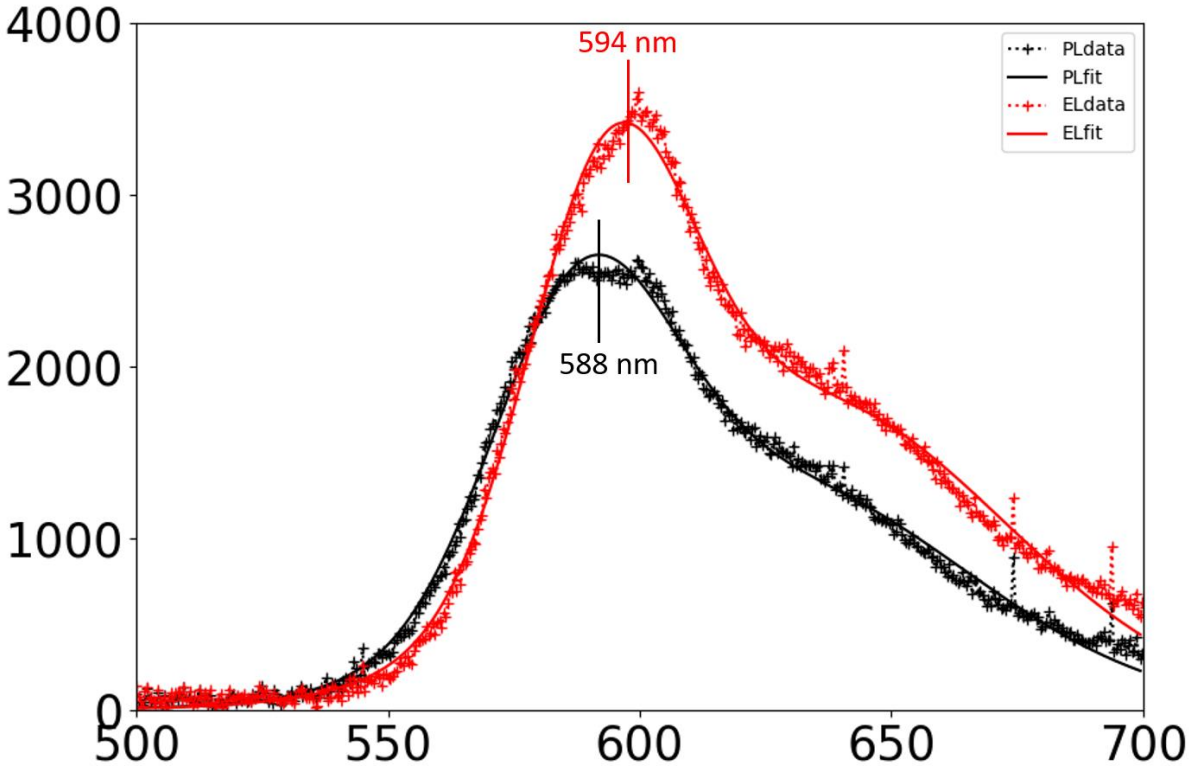

Figure A.1. Fit of the EL and PL spectra of MEH-PPV. A double Gaussian curve was used to fit the spectra.

A.2 FTIR spectra

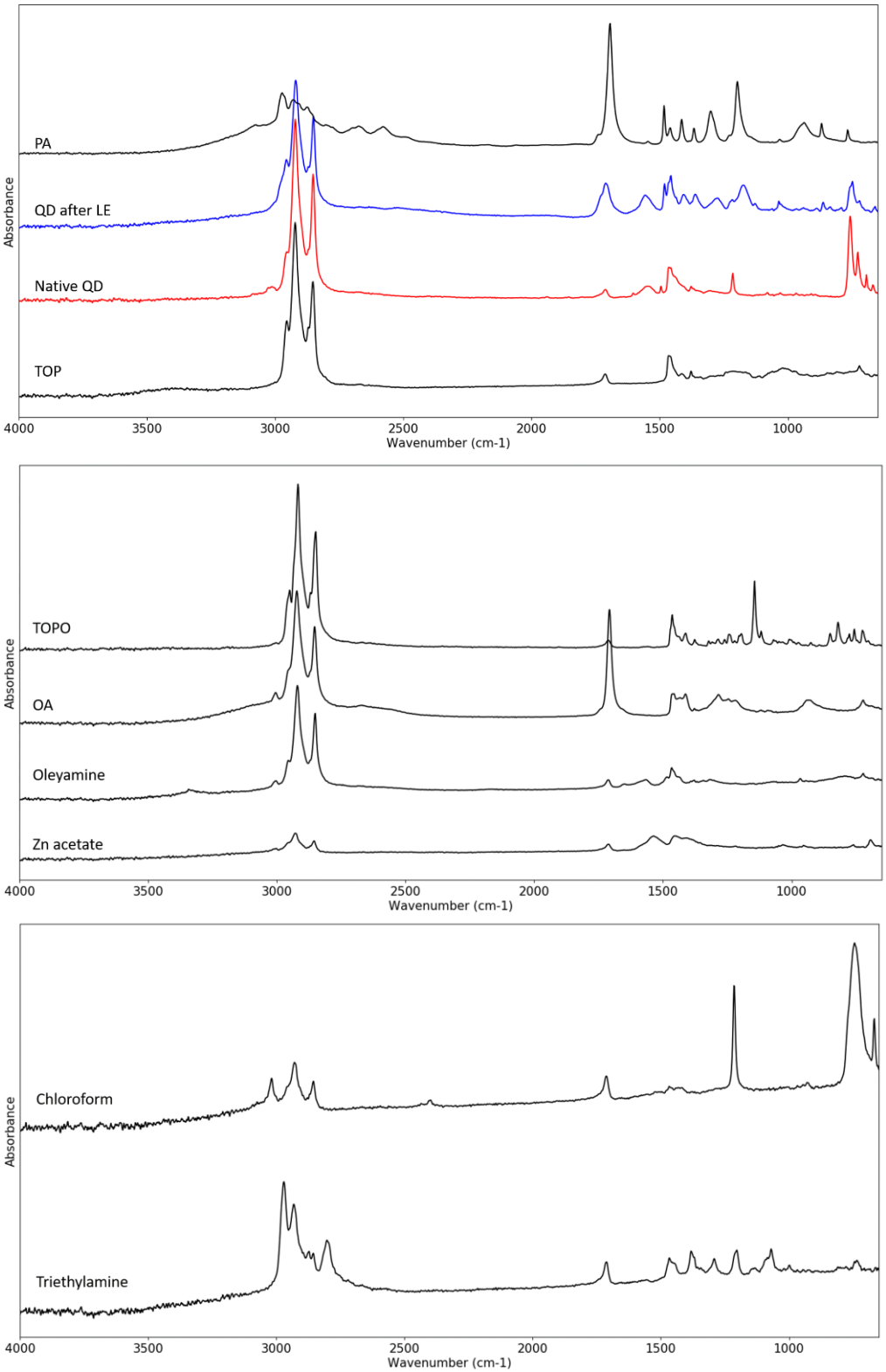

Figure A.2. FTIR spectra of all the non-toxic compounds that could be present on the surface of the QDs or in solution in the mixture that was obtained after the synthesis and ligand exchange procedure.

A.2 Theoretical potential profile equations in the EDL

The following equations were used to calculate the Debye length that was then used to predict the theoretical potential profile in the EDLs

For an electrolyte solution:

$$\boldsymbol{L_D = \sqrt{\frac{\varepsilon_r \varepsilon_0 k_B T}{2 * 10^3 N_A q^2 I}}} \quad \textbf{(A.1)}$$

For a doped semiconductor:

$$L_D = \sqrt{\frac{\varepsilon_r \varepsilon_0 k_B T}{N_{dop} q^2}} \quad \textbf{(A.2)}$$

Where L_D is the Debye length, $\varepsilon_r * \varepsilon_r$ is the dielectric constant of the medium, k_b is Boltzmann's constant, T is the temperature, q is the elementary charge, N_A is Avogadro's number, I is the ion concentration and N_{dop} is the doping density.